Nanoscale Engineering of Heterostructured Anode Materials for Boosting Lithium-Ion Storage

Gen Chen, Litao Yan, Hongmei Luo, and Shaojun Guo**

Rechargeable lithium-ion batteries (LIBs), as one of the most important electrochemical energy-storage devices, currently provide the dominant power source for a range of devices, including portable electronic devices and electric vehicles, due to their high energy and power densities. The interest in exploring new electrode materials for LIBs has been drastically increasing due to the surging demands for clean energy. However, the challenging issues essential to the development of electrode materials are their low lithium capacity, poor rate ability, and low cycling stability, which strongly limit their practical applications. Recent remarkable advances in material science and nanotechnology enable rational design of heterostructured nanomaterials with optimized composition and fine nanostructure, providing new opportunities for enhancing electrochemical performance. Here, the progress as to how to design new types of heterostructured anode materials for enhancing LIBs is reviewed, in the terms of capacity, rate ability, and cycling stability: i) carbon-nanomaterials-supported heterostructured anode materials; ii) conducting-polymer-coated electrode materials; iii) inorganic transition-metal compounds with core@shell structures; and iv) combined strategies to novel heterostructures. By applying different strategies, nanoscale heterostructured anode materials with reduced size, large surfaces area, enhanced electronic conductivity, structural stability, and fast electron and ion transport, are explored for boosting LIBs in terms of high capacity, long cycling lifespan, and high rate durability. Finally, the challenges and perspectives of future materials design for high-performance LIB anodes are considered. The strategies discussed here not only provide promising electrode materials for energy storage, but also offer opportunities in being extended for making a variety of novel heterostructured nanomaterials for practical renewable energy applications.

1. Introduction

The ever-fast energy consumption in our day-to-day life has led to rapid depletion of fossil fuels. The critical energy crisis and environmental pollution associated with the usage of non-renewable resources have stimulated an outcry for supply of clean energy.[1] People are now seeking new opportunities from the solar and wind energy, which are regarded as environmentally friendly and clean energy. However, these energies are not stable in nature and cannot be directly applied as a power supply in the grid, bringing energy storage and conversion on request. Electrochemical energy storage (EES) devices such as lithium-ion batteries (LIBs) have been extensively explored and applied in many fields. They provide the dominant power source for a range of devices, including portable electronic devices and electric vehicles, due to their long lifespan and high energy and power densities. Novel LIB devices are considered to be a promising option in the quest to alleviate the problems associated with the rapid depletion of fossil fuels and the deterioration of the global eco-environment.[2] Rapid growth of LIBs is a microcosm of the rapid development of EES, reflected by the fast electric-vehicle (EV) market growth.[3] However, the current LIBs as a power supply for EVs is not satisfactory enough in terms of capacity, cost, and lifetime. The US Department of Energy's EV Everywhere Grand Challenge[4] sets a target range of 250–300 miles per charge for the next generation of electric-driven cars, placing great pressure on the vehicles' battery packs. Meanwhile, the costs need to be cut from $350–550 per kWh to $125 per kWh, and battery lifespan needs to be extended to 15 years from its current 8 years to gain meaningful market share.

Therefore, the interest in exploring new anode materials for LIBs has been drastically increasing due to the surging demands for clean energy and great market potential. However, the electrochemical performances of these developed anode materials may be not as good as anticipated due to their challenging issues, such as quickly fading capacity, poor conductivity, large volume expansion, solubility into electrolyte, and

Dr. G. Chen, L. Yan, Prof. H. Luo
Department of Chemical and Materials Engineering
New Mexico State University
Las Cruces, NM 88003, USA
E-mail: hluo@nmsu.edu

Prof. S. Guo
Department of Materials Science & Engineering
Department of Energy & Resources Engineering
College of Engineering
Peking University
Beijing 100871, China
E-mail: guosj@pku.edu.cn

DOI: 10.1002/adma.201600164

large voltage hysteresis between charge and discharge, aggregation, etc., which strongly hinder their further practical applications. This has been particularly shown in silicon anode materials with high theoretical capacity of over ca. 4000 mA h g^{-1}, but their huge volume change of ca. 400% will necessarily lead to lattice stress and, consequently, the structure deterioration during charge and discharge (lithiation/delithiation) processes.[5] Conversion/alloy transition-metal compounds (A_xB_y, A = Fe, Co, Ni, Sn, Mn, Mo, etc.; B = O, S, N, etc.[6,7]) are promising as electrode materials with advantages such as low cost, ease of synthesis, and environmental friendliness. Unfortunately, these compounds normally suffer from poor conductivity and large voltage hysteresis in addition to the remarkable volume change upon lithium-ion insertion and extraction, making their commercial availability restricted.

Over the past decade, tremendous efforts have been paid to solving the aforementioned problems, which can be mainly categorized into the following two main streams: i) making nanostructures with well-controlled size, shape, and structure to optimize the utilization of active materials; ii) designing heterostructures by coupling carbon and polymer-based additives with electrode materials to enhance the structural stability and conductivity, and thus improve electrochemical performance. Various nanosized anode materials with complexity have been thoroughly investigated through in-depth experiments and theoretical simulations. The relationship between the composition, morphology, surface property, porosity, and thermal stability of these nanomaterials and their electrochemical performances has been comprehensively revealed, leading to further understanding of the intrinsic electrochemical behavior. Strategies and progress in fabricating nanostructured anode materials for LIBs have been summarized and thoroughly discussed in some recent prominent reviews, including the topics of carbon-based electrode materials (e.g., three-dimensional graphene-based composites,[8] porous graphene materials,[9] electrospun carbon nanofibers[10]), transition-metal-based oxides or sulfides,[11] or other general topics on nanomaterials.[12–14] However, all these mentioned reviews paid limited attention to the emerging and urgent engineering and synthesis of heterostructures, especially those developed in very recent years.

The most recent intriguing research on LIB anode materials has been directed toward rational design and fabrication of heterostructures for boosting lithium-ion storage. With the concept of "materials design", the special structural control of heterostructures enables superior electrochemical properties, such as enhanced conductivity, stability, and improved capacity, over their single counterpart. Briefly, heterostructured anode materials are integrated by two or multiple components with readily controlled shape and morphology. In addition to the advantages inherited from the reduced size, their excellent electrochemical performance is also attributed to the reinforcement and synergetic effect from multiple components. Moreover, each of the components can be easily engineered or substituted, which therefore offers versatile opportunities to optimize the electrochemical properties. Heterostructured anode materials are often associated with significantly enhanced structural stability during cycling, even at high current densities, comparing with single or simply mixed components, which can be ascribed to their "self-protected" nature in terms of confined reaction space, suppressed dissolution of active materials, and accommodated volume variation.

Here, we highlight recent advances in the design and exploration of highly promising heterostructured anode materials for boosting lithium-ion storage. Before we look into the topic of

Gen Chen obtained his Ph.D. in 2016 in chemical engineering at New Mexico State University with research interest in the nanoscale engineering of heterostructured composites for energy conversion and storage. He received his B.E. (2009) and M.S. (2012) in materials science from the Central South University. He started his Ph.D. program in the fall of 2012 and joined Los Alamos National Laboratory as a visiting researcher (2014–2015).

Hongmei Luo received her B.S. (1992) in chemistry from Fuyang Normal University, China, and Ph.D. (2006) in chemical engineering from Tulane University. She was a postdoctoral research associate at Los Alamos National Laboratory from 2006 to 2009 and she joined the Chemical and Materials Engineering Department at New Mexico State University in fall, 2009. She was promoted to Associate Professor in 2014. Her group research focuses on epitaxial thin films for magnetic and superconducting properties and nanostructured materials for energy applications.

Shaojun Guo is currently a Professor of Materials Science and Engineering with a joint appointment at the Department of Energy & Resources Engineering, at the College of Engineering, Peking University. He received his B.Sc. in chemistry from Jilin University (2005) and his Ph.D. in analytical chemistry from the Chinese Academy of Sciences (2011) with Profs. Erkang Wang and Shaojun Dong, and then joined Prof. Shouheng Sun's group as a postdoctoral research associate from January 2011 to June 2013 at Brown University. His research interests are in engineering nanocrystals and 2D materials for catalysis, renewable energy, optoelectronics, and biosensors.

heterostructures, a very short review of recent work on the development of nanosized anode materials for LIBs will be firstly presented in order to clarify what the current trends are in the synthesis and utilization of advanced electrode materials for LIBs. The disadvantages of these nanostructures for LIB application are accordingly discussed. Then, the most recent progress in the design and fabrication of heterostructured electrode materials is highlighted, covering the following new strategies for advanced heterostructures: i) carbon-materials-supported heterostructured electrode materials, taking advantage of the intrinsic high electronic conductivity, the high surface area, and the tunable porous structure of carbon; ii) conducting-polymer-coated electrode materials, in which the conducting polymer is featured with light weight, large capacitance, good electric conductivity, ease of synthesis, and low cost; iii) transition-metal compounds with core@shell structure, making the use of both components and offering better electrochemical properties over their single counterparts through the synergistic effect; iv) combined strategies to make novel, more complex heterostructures, offering the comprehensive characteristics as mentioned above. By employing these different strategies, nanoscale heterostructured anode materials with reduced size, large surface area, excellent electrical conductivity, structural stability, and fast electron and ion transport, have been successfully designed and prepared for boosting LIBs in terms of high capacity, long cycling lifespan, and durability at high rate. We finally look into the challenging issues and perspectives of these selected topics. This review prompts the nanoscale engineering and conceptual design of advanced heterostructures for efficient lithium-ion storage, which will appeal to the scientific communities who are interested in the general areas of physical chemistry, electrochemistry, energy science, nanomaterials and nanotechnology, and electroanalysis.

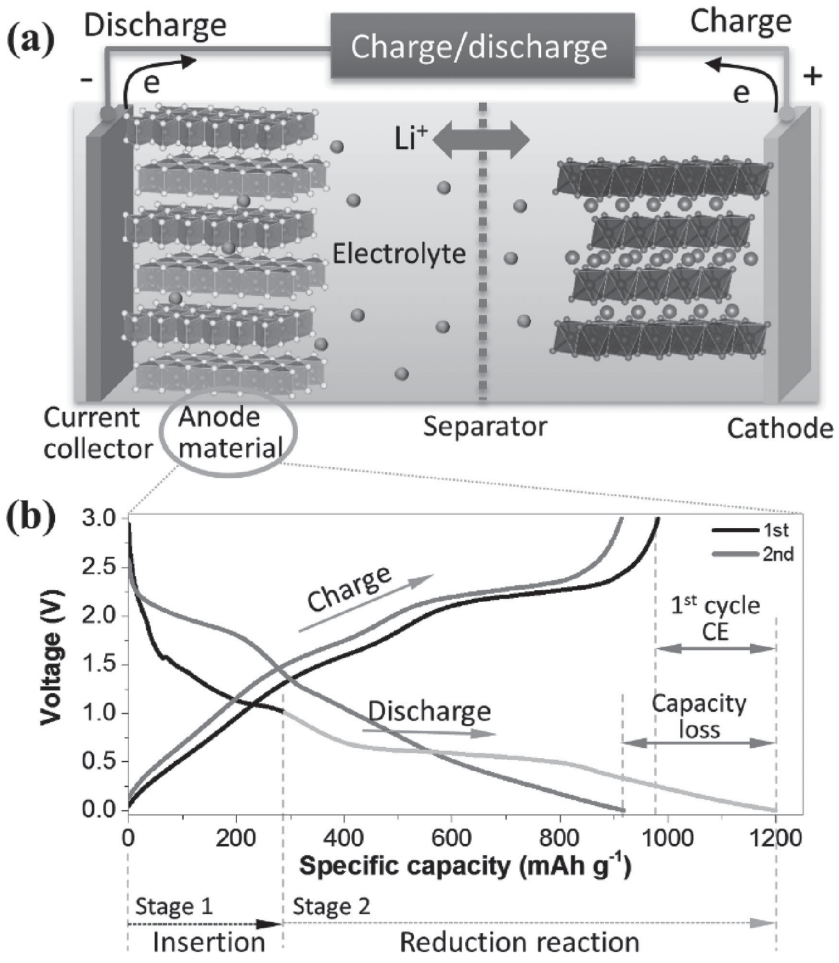

Figure 1. a) Schematic configuration and working principles for conversion-/alloy-reaction-based LIBs (layered MoS_2/lithium-salt electrolyte/$LiCoO_2$). b) Typical charge/discharge profile of conversion-/alloy-reaction-based anode materials (obtained on a half-cell test, in which lithium metal is typically applied as counter electrode).

2. Electrochemistry of LIBs

As a major part of EES, LIBs with high energy and power densities have attracted worldwide interest due to their important role as the dominant power sources for portable electronics, electric vehicles, hybrid vehicles, and large-scale electrical grids.[15] LIBs are composed of a negative electrode (anode), a separator, an electrolyte, and a positive electrode (cathode) in configuration.[13,14] In principle, the energy storage in LIBs depends on the reversible electrochemical reactions/charge storage in the electrode materials, strongly associated with electron and ion transport as shown in **Figure 1**a. During the discharge process, electrochemical reactions take place at the electrodes, and the generated electrons flow through an external circuit to drive the external load. During the charge process, an external voltage is applied to store electrons at the electrodes by reversible electrochemical reactions. The ions diffuse between the electrodes through the electrolyte, while the electrons flow through the external circuit. The high energy density of LIBs can be partially realized by using conversion- or alloy-reaction-based anodes materials with high specific capacity. The power density of LIBs is another important prerequisite for their versatile applications, and strongly depends on the kinetics of the electrodes. Tuning the electrode materials at the nanoscale will benefit the kinetics from the increased active reaction sites and interfaces, and lead to a reduced diffusion path for lithium-ion intercalation and deintercalation, described as:[16]

$$\tau = L_{ion}^2 / D_{ion} \quad (1)$$

where τ is ionic diffusion time in the host material, L_{ion} is the ionic diffusion length, and D_{ion} is the ionic diffusion coefficient. For a given material, D_{ion} is similar to and τ grows quadratically with L_{ion}. Nanostructured anode materials can provide

a large electrode–electrolyte contact area, and the lithium-ion diffusion time can be reduced greatly when the ionic diffusion length is shortened; this facilitates the complete utilization of the active materials at high current density. Nevertheless, nanomaterials for LIBs can be double-edged due to the decreased packing density, which leads to low volumetric energy density and unfavorable structural stability due to the large and highly active surface.

Generally, non-aqueous liquid electrolytes are prepared by dissolving a lithium salt in a mixture of organic carbonate solvents. During the first discharge, the decomposition of the electrochemically unstable solvents and salt near the anode surface will take place upon the electron transfer. Side reactions promote the formation of inorganic compounds (e.g., LiF, Li_2O, and Li_2CO_3), and organic species (e.g., lithium ethylene dicarbonate) and many others including oligomeric and polymeric compounds, which deposit on the electrode surface and form a multicomponent solid electrolyte interphase (SEI) layer.[17,18] The behavior of fast charging on ionic transfer across the electrode–electrolyte interface has been demonstrated as diffusion-controlled by both experiment and modeling.[19] Similar to graphite, if the lithium ions for the charge-transfer reaction at the interface of the anode/SEI layer exceed the lithium ions that are reacted with or diffused into the nanoparticles, they may be deposited at the interface of the anode and the electrolyte during charging, which would consequently lead to the dendritic growth of Li.[20] The potential safety issues apart, the formation of Li deposits may consume the lithium ions needed for the electrochemical reaction, and this is responsible for the degradation in performance of LIBs.[13] Simultaneously, the formation of the SEI layer on the anode–electrolyte interface will also consume the electrolyte, leading to irreversible capacity loss. However, a stable SEI layer is essentially important for a healthy battery cell, due to the following three reasons. Firstly, an effective SEI layer helps maintain the chemical and mechanical stability of the electrode; secondly, it further hinders the trapping of lithium ions and prevents decomposition of the electrolyte at the electrode–electrolyte interface; thirdly it allows lithium ions to pass freely and passivates the electrode surface to reduce undesired side reactions.[17] Conversion-/alloy-reaction-based anode materials generally involve a huge volume change during the charge and discharge processes, which will necessarily result in a repeated SEI layer formation and therefore fast capacity fading.[21] These general considerations principally provide the guidance for the design and fabrication of novel anode materials.

The typical charge/discharge profile of a conventional anode material for the first 2 cycles is presented in Figure 1b. The initial discharge and charge capacities can be determined based on the weight of the active materials. The corresponding Coulombic efficiency can be also calculated by the ratio of the 1st charge capacity to the discharge capacity. The irreversible capacity loss (difference between discharge and charge capacities) in the 1st cycle is mainly attributed to the formation of the SEI layer. Efficient anode materials can be reflected by the high Coulombic efficiency and low irreversible capacity loss. For redox-reaction-based anode materials, two typical processes including the insertion of lithium ions and a reduction reaction are generally involved in a discharge period. The major contribution to the high theoretical capacity is the redox reaction, which involves transfer of multiple electrons. The charge process reversibly corresponds to the discharge process with a platform at different potentials, reflecting the voltage hysteresis. The performance of LIBs is mainly determined by the electrode material, which lies at the heart of the research field. Novel electrode materials play a significant role in the efficient and effective use of energy. Hence, the development of EES is largely attributed to the development and innovation of new electrode materials with tailored structure and high performance.

As mentioned above, transition-metal compounds are found to be promising as anode materials due to their high theoretical capacity based on conversion redox reactions, involving multiple electron transfer per unit metal atom:

$$A_aB_b + (b \times n)Li^+ + ae^- \leftrightarrow aA + bLi_nB \quad (R1)$$

The category of transition-metal compounds is very popular because of their high theoretical capacity and natural abundance. However, there are also some demerits during the redox reaction. For instances, the formation of the lithium ion from Li_2O is a thermodynamically unfavorable process, strongly hindering the reversibility. The product, such as Li_2S, is very reactive with the electrolyte, forming the undesired SEI on the surface of the electrode material, and thus affecting the cyclic stability and rate capability. Meanwhile, the Coulombic efficiency of charge to discharge is not as good as that of graphite. Large volume variations during lithiation and delithiation may lead to the pulverization and deterioration of the material structure. Other anode materials, such as silicon, suffer from similar demerits with even larger volume expansion and contraction. In this regard, considerable efforts have been paid into manipulating the nanostructures of electrode materials to overcome the difficulties associated with their huge volume change, poor conductivity, and large polarization, etc.

3. Nanostructured Anode Materials

Battery performance, including rate and cycling capacities, is heavily dependent on material properties, such as theoretical capacity, electronic conductivity, and reversibility. Except for the intrinsic properties of electrode materials, the particle sizes and morphologies of materials also affect battery performance. Reducing the materials size to the nanoscale can provide a good opportunity to enhance LIB performance by improving the lithium-ion diffusion and the contact area between the electrolyte and the electrode. Furthermore, the volume change during the charge/discharge processes can be accommodated by the created space in the special nanostructure. With the rapid advances of materials design strategies and synthetic techniques, remarkable progress has been achieved in the preparation of nanostructured anode materials. It has been repeatedly demonstrated that superior electrochemical performance is delivered over the bulk counterparts because of the unique properties associated with decreased size, large surface area, and favorable morphology.[13,22–25] Our recent work confirms that smaller $TiNb_2O_7$ nanoparticles (ca. 10 nm) display better lithium-ion-storage properties (higher specific capacity, rate

performance, and cycle performance) than the larger $TiNb_2O_7$ (ca. 100 nm).[26] Compared with bulk materials, nanomaterials with non-regular morphology have proven to deliver better performance in LIBs, but their performance including rate and cycle durability is still limited by various factors, such as volume expansion and cracking of nanoparticles caused by fast repeated lithium-ion insertion/extraction.[13,24,25] Besides, the high packing density of the electrode caused by a non-regular morphology can limit kinetic diffusion through the nanoparticle layers. Moreover, the secondary reactions, including electrolyte decomposition and the formation of SEI films at the interface between the electrodes and electrolyte, can become more serious since the high surface area of the nanoparticles allows them to access the electrolytes more easily.[27]

To date, numerous nanostructures have been developed for LIBs as summarized partially in **Figure 2**. To start with, one dimensional (1D) nanostructures, including nanowires and nanorods, can overcome some of the disadvantages of nanoparticles, which has been well demonstrated in the use of silicon nanowires.[29] They displayed an overall capacity as high as 3541 mA h g^{-1}, which was maintained as constant up to 10 cycles at the low current density of 0.05 C. Such high performance of silicon nanowires for LIBs can be ascribed to the fact that the 1D nanostructure can restrict the structural disintegration between the electrode and the current collector due to huge volume changes of 400% for the bulk silicon during the cycling tests, and also can provide the directional electronic/ionic transportation pathways. Moreover, the 1D nanostructure can provide excellent mechanical stability over several cycles of lithium-ion insertion and extraction. Inspired by these particular merits of 1D nanostructures, several methods, such as the hydrothermal route,[39] electrodeposition,[40] the thermal evaporation process,[41] electrospinning,[42] and chemical vapor deposition (CVD) techniques,[43] have been employed to fabricate new 1D nanostructures. Recently, α-Fe_2O_3 nanorods[39] prepared by the hydrothermal method were found to deliver a capacity as high as 1275 mA h g^{-1} after 30 cycles at 0.1 C, and maintain a capacity of 916 mA h g^{-1} after 100 cycles at 1 C.

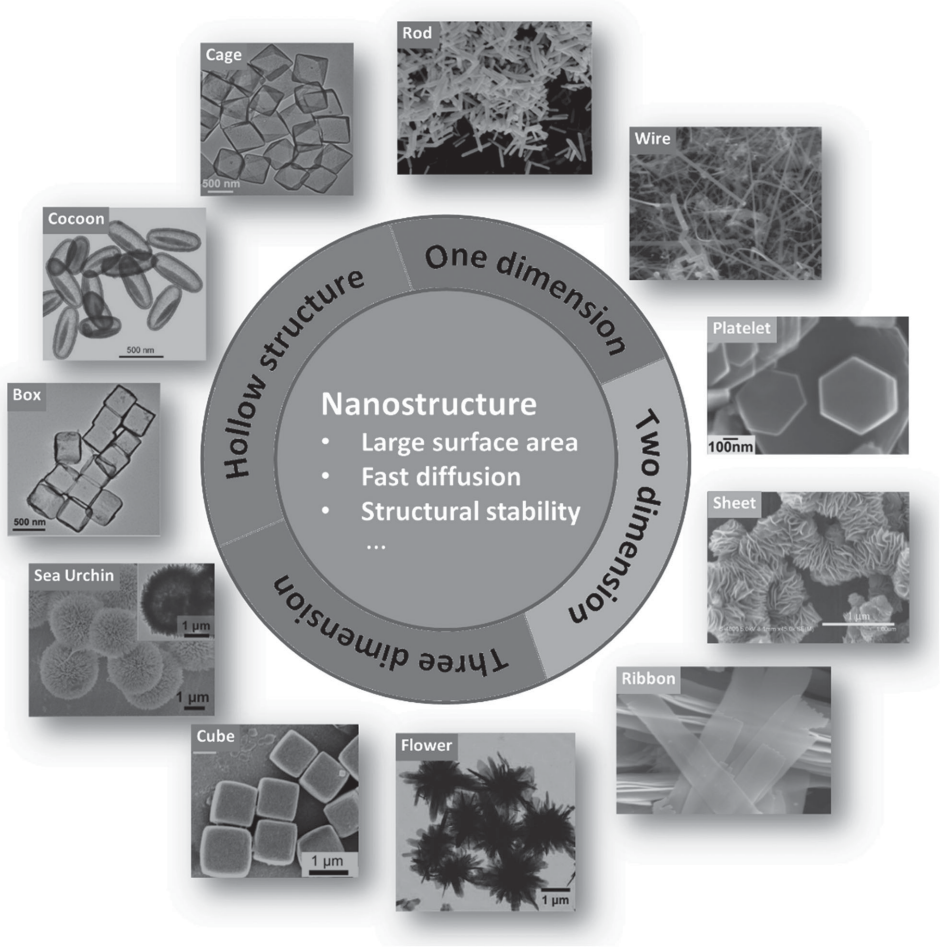

Figure 2. Nanostructured anode materials for LIBs. 1D nanorods[28] and nanowires;[29] 2D nanodisks,[30] nanosheets,[31] and nanoribbons;[32] 3D nanoflowers,[33] and nanocubes;[34] hollow sea-urchin-like structure,[35] nanoboxes,[36] nanococoons,[37] and nanocages.[38] Adapted with permission: nanorods: ref. [28], Copyright 2011, and nanoboxes: ref. [36], Copyright 2011, American Chemical Society; nanowires: ref. [29], Copyright 2008, nanodisks: ref. [30], Copyright 2012, and sea-urchin structure: ref. [35], Copyright 2015, Nature Publishing Group; nanosheets: ref. [31], Copyright 2015, nanoribbons: ref. [32], Copyright 2015, and nanoflowers: ref. [33] Copyright 2012, Royal Chemical Society; nanocubes: ref. [34], Copyright 2015, nanococoons: ref. [37], Copyright 2007, and nanocages: ref. [38], Copyright 2012, John Wiley & Sons, Inc.

Besides, Fe_3O_4,[44] Co_3O_4,[45] and other metal oxides[46] with a new 1D structure also exhibited the high rate performance and high cycle durability, indicating that metal oxide anode materials with a 1D nanostructure can be good candidates as high-energy and high-power electrode materials for LIBs. The electrospinning method is another general technique to prepare a 1D nanostructure. $ZnCo_2O_4$ nanotubes[47] can be prepared by the electrospinning technique followed by thermal-annealing treatment of as-spun nanofibers in air. These special 1D nanostructures, comprising both interconnected nanocrystals and many nanopores in the tube walls, deliver relatively high capacity and cyclability.

Recent research has demonstrated that two-dimensional (2D) layered nanostructures (nanosheets, nanoplatelets, nanodisks, nanoribbons, etc.) also show remarkably improved electrochemical performance compared to their bulk counterparts, since they provide large surface areas, enhanced open-edge morphologies, and finite lateral size.[48] MoS_2 nanosheets,[49] prepared by a facile hydrothermal method, exhibited high electrochemical performance for LIBs since their special structure can be beneficial for electrode kinetics.[50] Besides, metal oxides with structure characterized by mesoporous or nanoporous disks and nanosheets have also been extensively investigated as electrode materials for LIBs.[51,52] For instance, disk-like nanoporous Fe_2O_3 was demonstrated to have significantly enhanced capacity retention due to the highly exposed surface and pores.[53] Recently, we developed a one-step polymer-assisted chemical solution method for the synthesis of 2D V_2O_5 and manganese-doped V_2O_5 nanosheets.[54] The as-prepared V_2O_5 nanosheet with carbon coating exhibited a high capacity of about 300 (as cathode) and 600 mA h g^{-1} (as anode) at a current density of 100 mA g^{-1}. This unique network structure provides an interconnected transportation pathway for lithium ions, resulting in an improved rate and cycling performance.

Three-dimensional (3D) structures such as nanoflowers, nanocubes, or a sea-urchin-like structure can be easily derived from 2D nanosheets, 1D nanowires, or 0D nanoparticles. Unique hierarchical V_2O_5 nanoflowers[55] composed of many nanoparticles were prepared by a fast electrochemical reaction of vanadium foil in an aqueous NaCl solution followed by heat treatment. Such hierarchical nanoflowers provide the porous channels, facilitating fast lithium-ion diffusion and balancing the volume change during cycling process. They delivered high reversible specific capacities of 275 mA h g^{-1} (as cathode) with 100% Coulombic efficiency. Nanoflowers for high-performance LIBs can not only be evolved from 1D nanoribbons, but also derived from nanowires and 2D nanosheets. 3D Co_3O_4 nanoflowers and hyperbranched bundles[56] composed of large numbers of porous nanowires with lengths in the range of micrometers were developed for LIBs. SnS nanoflowers[33] consisting of a hierarchical arrangement of nanosheet subunits surrounding a central core were also employed as high-performance anodes for LIBs. Self-stacked CoO nanodisks[51] with 3D architecture deriving from the 2D nanosheets took the advantageous combination of small nanoparticles (0D), ultrathin, mesoporous, and large-area 2D nanosheets, and the self-stacked 3D structure, resulting in high rate and cycle performance. MoS_2 nanoflowers[57] represent another successful illustration of building a 3D structure by assembly of nanosheets.

Nanomaterials with a hollow structure are developed for LIBs because they not only deliver higher specific capacities but also provide better retentions and superior high-rate performances compared with their solid counterpart. Fe_2O_3 nanotubes[58] were demonstrated with a capacity of 391 mA h g^{-1} at a current density of 10 A g^{-1} after 1000 cycles. Recently developed Fe_3O_4-nanotube anode materials can retain their capacity of over 1000 mA h g^{-1} for 50 cycles.[23,58] Similar to iron oxides, SnO_2 with a hollow structure[59] has also been extensively investigated as the anode for high-performance LIBs. SnO_2 hollow nanospheres[60] can significantly prolong the cycle life of SnO_2, compared with pristine nanoparticles. They can deliver a capacity of 700 mA h g^{-1} after 30 cycles, while there is no capacity for pristine nanoparticles after several cycles. SnO_2 nanoboxes[36] and nanococoons[37] were also proved to have enhanced capacity and cycle performance. These transition-metal oxides with hollow structure have been applied as anode materials for LIBs because the unique structure not only balances the volume variation during the lithium-ion insertion/extraction process but also avoids the severe aggregation of the active materials.[61] Even more importantly, the large specific surface area of the hollow structure can provide a high specific capacity and high-rate performance due to the favorable reaction kinetics of lithium ions.

Admittedly, controlling the morphology of nanomaterials can effectively improve the electrochemical reaction efficiency for improved energy and power densities. However, they still suffer from poor conductivity, large volume change, and severe aggregation during the lithium-ion insertion/desertion process, which strongly limits their rate ability and cycling stability. The fabrication of heterostructured nanomaterials with special structures is therefore of irreplaceable importance because it may provide additional advantage for next-generation LIBs. The remarkable advances on how to obtain novel heterostructured materials and how they affect the electrochemical performances are discussed in the following sections.

4. Nanoscale Engineering of Heterostructured Anode Materials for Boosting Lithium-Ion Storage

Increasing attention has been paid to fabricating heterostructured electrode materials for advanced LIBs owing to their special features, such as high surface area, enhanced structural stability, short lithium-ion diffusion path length and high electron-transportation rate. Moreover, heterostructures may provide the unique properties of stable SEI formation, confined electrochemical reaction space, synergetic effect, and interfacial storage capacity, etc., offering the additional opportunity for delivering better lithium-ion-storage ability. These advantages have driven researchers to explore new methods for novel heterostructured anode materials for highly efficient lithium-ion storage, which can be summarized into the follow aspects:[7,13,62] i) the fabrication of conductive-carbon-supported nanostructured anodes with novel morphologies, including hollow spheres,[63] nanorods,[64,65] spindles,[66] and nanotubes[67] ii) making conductive-polymer-coated electrode materials for greatly improving the conductivity and accommodating the volume change and strain;[68] iii) synthesis of inorganic core@shell structures by taking advantage of the synergistic effect

from the two components over their single counterpart;[13,69] iv) the combination of two or more above-mentioned approaches. As the field is growing very quickly, the most recent developments and advances on the engineering of heterostructured electrode materials on the nanoscale will be deliberated in this review.

4.1. Carbon-Materials-Supported Heterostructured Electrode Materials

Supporting carbon materials show great potential for electrochemical energy conversion and storage applications because they exhibit several interesting properties, including high electrical conductivity, excellent stability, large surface area, and tunable porous structure, etc. To date, a variety of carbon-based materials, such as graphene, carbon nanotubes (CNTs), porous carbon, etc., have been widely applied as either supporting or conducting agents in electrodes for much improved LIB performances in terms of stability and capacity. Graphene or CNTs are normally utilized in a direct way to form an integrated electrode, for reducing the resistance and stabilizing the formation of the SEI. For porous carbon, the tunable porosity (pore connectivity, length, and pore-size distribution) can introduce an additional factor for enhancing LIBs by facilitating ion diffusion/mass transfer. However, all the mentioned carbon materials still lack sufficient lithium-ion capacity due to their intrinsic storage mechanism. Therefore, the combination of nanostructured anode materials and different forms of carbon materials can provide new insights into the enhancement of the LIB performance.[70–73]

4.1.1. Porous Carbon

The most recent research has revealed that loading metal compounds or other elementary substance onto porous carbon is an effective and efficient way to improve the overall performance of electrode materials. Sulfur is very promising as one of the next-generation high-energy-density batteries because of its high theoretical capacity as well as low cost and earth abundance, etc. Nevertheless, its practical use is greatly hindered by its intrinsic low conductivity and dissolvability in an electrolyte. Therefore, the porous carbon matrix with hierarchical pore structure has been intensively applied in lithium–sulfur batteries because the porous carbon can enhance the conductivity, prevent the dissolution of intermediate lithium polysulfide into the electrolyte, and accommodate the large volume expansion during cycling. 3D interconnected porous carbon aerogels were successfully applied as a sulfur immobilizer for sulfur impregnation,[74] showing high rate and cycling stability. The multiple functions enable the achievement of either high capacity or superior stability over the sulfur single component. Another typical case is the application of porous carbon in silicon-based LIBs. Similar to sulfur, silicon delivers extremely an high theoretical capacity of 4000 mA h g^{-1}, but suffers from poor conductivity and large volume change during the electrochemical reaction. Confining the redox reaction of silicon in the porous carbon matrix hugely accommodates the volume change and maintains the original structure. The large surface area also ensures efficient contact between the electrolyte and the active material. A high reversible capacity of 1050 mA h g^{-1} even at a high current density of 10 A g^{-1} was proved through the combination of porous carbon with silicon particles.[75] With the merits from the porous carbon nanostructure, not only have silicon and sulfur batteries with promising electrochemical performances been successfully developed, but also EES devices based on phosphorus and transition-metal compounds have been achieved, with excellent battery properties. Elementary phosphorus has quite a low molecular weight and therefore a high theoretical specific capacity. However, its insulating nature and its electrical inactivity renders its with very poor capacity retention. Porous carbon nanofibers have been used as new support for phosphorus for LIBs[76] with a high retention capacity of 990 mA h g^{-1} and no structural change after cycling.

Porous carbon can be intentionally engineered through the concept of "materials design" to achieve desirable heterostructures. Chemically synthesized mesoporous carbon with various morphologies and nanostructures has been applied as an efficient conductive agent, resulting in much improved electrochemical performance. For instance, a new 2D MoS_2/mesoporous carbon (MoS_2/m-C) hybrid nanoarchitecture with an ideal MoS_2/m-C atomic interface,[77] in which single-layer MoS_2 and m-C are sandwiched in an alternating sequence (**Figure 3**) was designed for enhancing LIBs. The sandwich-like structure was achieved by carbonization of the polymer molecules inserted into the MoS_2 layers. (Figure 3a,b). The different inserted species introduced a large layer spacing compared with bare MoS_2 nanosheets (Figure 3c–e). A superstructure of the as-prepared MoS_2/m-C hybrid nanosheets with alternating single layers can provide much larger atomic-interface contact/interaction between single-layer MoS_2 and single-layer carbon nanosheets than the traditional MoS_2/C nanocomposite with limited interface contact (Figure 3f). Such an architecture of layered MoS_2/m-C hybrids with alternating sequence offers advanced properties: i) improving the electrical conductivity of MoS_2, especially in the *c*-direction, ii) reducing aggregation and restacking of MoS_2 nanosheets, iii) accommodating volume expansion upon lithiation, iv) mitigating polysulfide shutting, and v) in particular, providing the largest interface contact for lithium-ion storage with an obvious synergetic effect between the single-layer carbon and the MoS_2 nanosheets. These benefits are readily attributed to the heterostructure. As a result, the as-synthesized MoS_2/m-C nanosheet superstructure exhibited a maximum reversible specific capacity of 1183 mA h g^{-1} at 200 mA g^{-1} with excellent rate capability (943 mA h g^{-1} at 6400 mA g^{-1}) and long cycle life (over 500 cycles). This concept was extended to make highly crystalline MoS_2 nanosheets with only a few layers (≤5 layers) anchored on 3D porous networks of carbon nanosheets.[78] The robust heterostructure offers the maximized surface-to-surface contact between the MoS_2 and carbon sheets, avoiding the aggregation of MoS_2 and improving the structural stability. Simultaneously, such a network ensures fast transport of both electrons and ions, leading to excellent electrochemical performances (676 mA h g^{-1} even after 520 deep cycles at 2 A g^{-1}). Similarly, ultrathin MoS_2 nanosheets supported on chemically synthesized N-doped carbon nanoboxes[79] was reported with excellent lithium-storage capability. All the interesting heterostructures take advantage of the

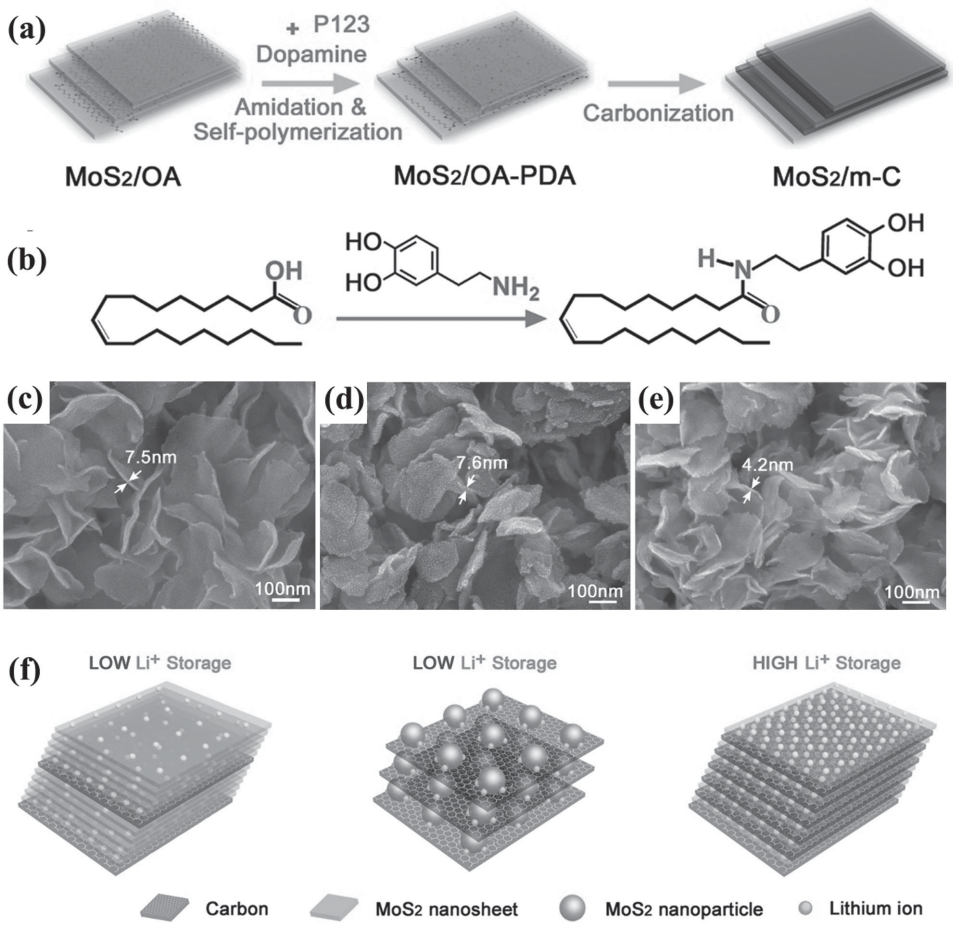

Figure 3. Synthesis process and morphology characterization of the MoS_2 /m-C nanosheet superstructure. a) Schematic illustration of the synthesis process. b) The amidation reaction of oleic acid (OA) and polydopamine (PDA). c–e) SEM images of the fresh MoS_2 nanosheets (c), the MoS_2/m-C nanosheet superstructure (d), and the annealed MoS_2 nanosheets (e). f) Schematic illustration of lithium-ion storage at the MoS_2/carbon atomic interface. The concept of the rational design of the MoS_2/m-C nanosheet superstructure for creating the ideal MoS_2/C atomic interface to enhance lithium-ion storage. Adapted with permission.[77] Copyright 2015, John Wiley & Sons, Inc.

improved conductivity through tight contact between the carbon and MoS_2 nanosheets and the strong interface synergistic effect, finally resulting in excellent LIB performance.

The porous structure with well-controlled porosity can be readily derived from blocking polymers such as poly(ethylene oxide)–poly(propylene oxide)–poly(ethylene oxide) (PEO–PPO–PEO), etc. The flexible nature of the polymer makes it possible to determine and modify the shape and morphology based on the active component. In our previous work, we reported a general polymer-assisted solution approach to grow transition-metal-oxide nanostructures with a porous carbon coating as anodes for LIBs.[80] The thin carbon layer was formed on the surface of the as-obtained nanoparticles after the carbonization of the polymer for enhancing the LIBs. However, for the intrinsic large volume change of certain materials during the electrochemical reaction, the carbon coating layer is subject to cracking when it undergoes the cycling processes. Through fabrication and design of state-of-the-art materials architectures, a novel structure of MnO nanoparticles confined in CNTs, with a peapod-like structure, was recently fabricated through self-polymerization of dopamine on the surface of MnO precursor nanowires (**Figure 4**).[81] The nanowires broke into short nanorods or nanoparticles during the high-temperature carbonization, creating 20.6% void space inside the CNTs (Figure 4a–c). Compared with MnO NWs (149 mA h g^{-1}) and MnO@C core@shell NWs (547 mA h g^{-1}), the engineered heterostructure exhibited a much higher specific capacity of 1119 mA h g^{-1} at 500 mA g^{-1}. The void space of the nanopeapods could accommodate the volume change, and therefore provide superior structural integrity over the fully filled materials (Figure 4d,e). No obvious morphology change was observed on the nanopeapod structure after 1000 cycles at a high rate of 2000 mA g^{-1}, indicating that transition-metal-oxides–CNT heterostructures are of great potential in stable energy storage. Another successful electrode design was recently reported, to make single silicon nanoparticles encapsulated into a conductive carbon shell,[82] leaving the void space for expansion and contraction during the electrochemical reaction.

The above important studies indicate that the integration of the configuration and arrangement of the active material with porous carbon can provide a general principle for the fabrication of heterostructured anode materials for advanced LIBs. The

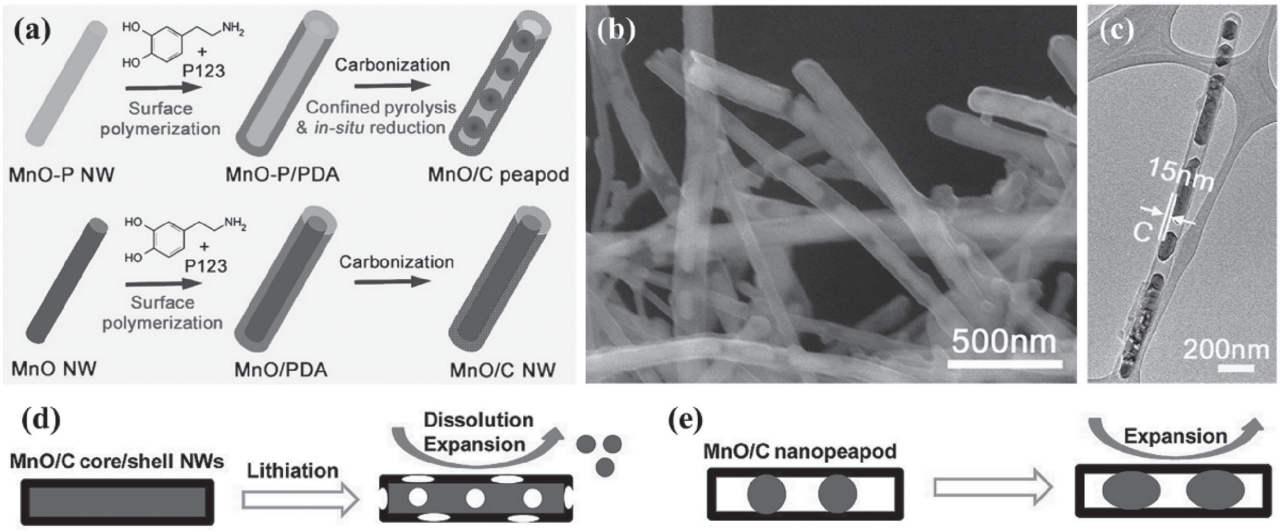

Figure 4. a) Schematic illustration on the preparation of the heterostructured MnO@C nanopeapods and MnO@C core@shell NWs. b–e) SEM image (b), TEM image (c), and schematic illustration of the structural stability of fully filled and partially filled MnO@C heterostructures (d,e). Adapted with permission.[81] Copyright 2015, American Chemical Society.

common features of such material design are that: i) an ensemble of nanoparticles is encapsulated by a carbon layer to act as an electrolyte barrier; ii) the SEI film remains stable and spatially confined; iii) the volume change during the lithiation and delithiation process is restricted in the "carbon reactor". Overall, from the viewpoint of synthetic methods, there will still be plenty of room for designing other complex porous-carbon-based heterostructures considering the ease of synthesis and high reproducibility of the polymer-precursor-assisted carbonization process.

4.1.2. Carbon Nanotubes

Carbon nanotubes, discovered by Iijima in 1991,[83] are of great interest in energy-storage applications due to their outstanding flexibility, high theoretical tensile strength and good conductivity. They bring free-standing electrodes into vision with promising applications for wearable devices. CNTs can be engineered into a 3D network on a large scale through simple synthetic strategies.[84,85] Highly robust, flexible, binder-free lithium-ion electrodes were fabricated based on interpenetrative nanocomposites of ultralong CNTs and other active components such as Nb_2O_5, V_2O_5, and TiO_2.[86,87] Such a robust composite network architecture can be used for high-performance flexible electrodes with high capacity, high rate capability, and excellent cycling stability. Nevertheless, the intrinsic structure of CNTs is perfect and well-sealed, hindering their electrochemical activity for energy storage and conversion. Generally, CNTs are applied in the electrodes after certain chemical modifications to introduce activation/defect sites. Our recent work has confirmed that the TiO_2 layer can be conformally coated on CNTs[88] and further transferred to TiON nanoparticles anchored on the CNTs. The robust structure delivered much higher electrochemical performance than the bare TiO_2 (TiON) counterpart. Loading active materials (metals, transition-metal compounds, alloys, silicon, etc.[65,85,89,90]) with high theoretical capacity onto CNTs is the most effective way to improve the electrochemical properties. By applying CNTs as a template or substrate, a variety of heterostructures can be achieved, with much enhanced capacity and durability.[24,72,91] These have been well demonstrated in the preparation of cylindrical MoS_2 directly grown on CNTs for LIBs without the use of any other additives via a microwave-assisted route.[92] A low-cost solution synthesis of one-dimensional hierarchical NiO nanosheets covering bamboo-like amorphous CNTs composites[93] (**Figure 5**) for boosting LIBs was also reported by using sulfonated polymeric nanotubes (PNTs) as both the template and carbon source by a low-temperature thermal carbonization. Ni nanosheets were firstly loaded onto the PNTs and then further converted to NiO@CNTs composites, exhibiting a high discharge capacity of 1034 mA h g^{-1} at a current density of 800 mA g^{-1}, and high stability after 300 cycles.

With advanced methodologies, CNTs can either serve as a substrate for the growth of an electrode material, or be filled with various inorganic nanomaterials. These synthetic strategies make it possible to form a unique heterostructure with confined materials in the hollow space. Such a heterostructure can greatly reduce the dissolution of active materials into the electrolyte, while the void space inside the tube can still accommodate the volume change. A novel material with silicon nanoparticles mechanically confined in CNTs[94] was reported (**Figure 6**), showing that the volume expansion (ca. 180%) of the lithiated silicon nanoparticles was strongly restricted by the wall of the CNTs. This robust structure greatly reduced the dissolution of silicon into the electrolyte, leading to a very high reversible capacity of 1671 mA h g^{-1}. Another typical example of a peapod-like heterostructure was reported by Schüth and co-workers,[95] wherein cobalt oxides (Co_3O_4) were confined exclusively in the intratubular pores of a CNT array. The particle size of the Co_3O_4 could be tuned in the range of 3–7 nm by varying the thickness of the carbon layer. The unique structure of this material significantly

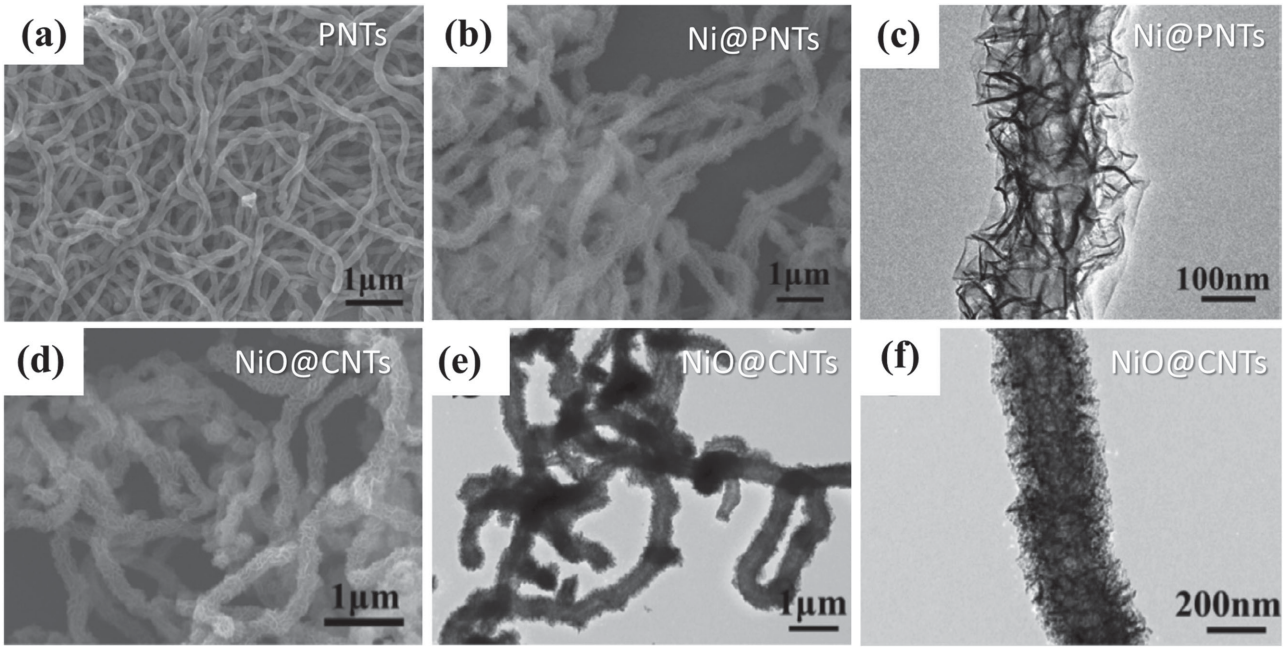

Figure 5. a) SEM image of the sulfonated PNTs template. b,c) SEM (b) and TEM (c) images of Ni-precursor@PNTs composites. d–f) SEM (d) and TEM (e,f) images of the NiO@CNTs composites. Adapted with permission.[92] Copyright 2015, Elsevier.

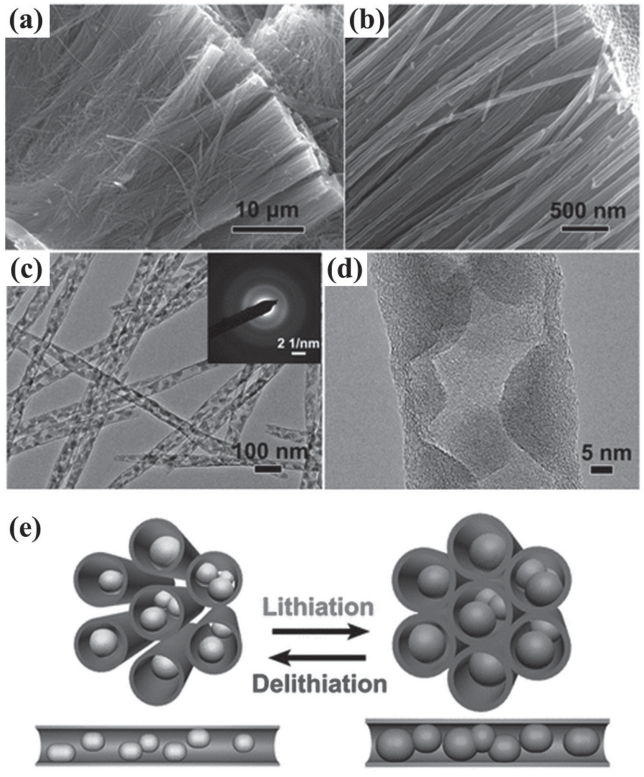

Figure 6. Microstructure of CNTs filled with silicon nanoparticles. a,b) SEM images, and c,d) low-magnification (c) and high-magnification (d) TEM images, clearly showing that the silicon nanoparticles are 100% filled inside the CNTs. The inset in (c) shows the selected-area electron diffraction (SAED) pattern; e) Illustration of the lithiation/delithiation of the CNTs filled with silicon nanoparticles. Adapted with permission.[94] Copyright 2015, American Chemical Society.

promotes the accessibility of the Co_3O_4 nanoparticles through mesopores, and facilitates fast lithium-ion diffusion transport by the network of CNTs. The Co_3O_4@CNT materials exhibited a high specific capacity of up to 781 mA h g^{-1} at a current density of 100 mA g^{-1} and excellent cycling performance. Different active materials, such as Sn,[96] Fe_2O_3,[97] and MnO_2,[98] etc., confined within CNTs, have been synthesized, demonstrating the robustness and high efficiency of such heterostructures for boosting LIBs.

Making CNTs into an interconnected 3D network or growing active materials on CNTs or confining them in the hollow space of CNTs are examples of state-of-the-art nanoscale engineering of heterostructures. A comparison between architectures of Fe_2O_3 nanoparticles confined in CNTs and Fe_2O_3 nanoparticles anchored on CNTs was carried out to explore better lithium-ion-storage materials.[99] The result revealed that the Fe_2O_3 nanoparticles confined in CNTs delivered a higher structural stability and integrity during the first charge and discharge cycle (**Figure 7**). Remarkable volume expansion and pulverization can be seen both cases, while the confined architecture provides significantly reduced deterioration in the structure. In principle, directly loading the active materials onto the surface of CNTs may not be effective due to uncontrolled conversion reaction space. Moreover, exposed nanoparticles on the surface of CNTs are subject to dissolution into the electrolyte, which is responsible for capacity degradation. The formation of an SEI layer on the exposed nanoparticles will be similar to the bare nanostructures with an unstable nature. Therefore, making the maximum use of the active material and achieving safe, stable, and high-capacity electrodes have always been radical challenging issues, and CNT-based heterostructures deserve constant attention in the community.

4.1.3. Graphene

Graphene is a one-atom-thick sheet of sp^2-bonded carbon atoms in a honeycomb crystal lattice with extraordinary electronic and mechanical properties. Since the first experimental investigation and exfoliation in 2004 by Geim, Novoselov, and co-workers[100] graphene has led to a decade of "graphene fever" in the field of materials science.[9,70,73,101,102] Graphene lies at the center of carbon-based materials for energy-storage applications. Novoselov et al. provided a general roadmap for graphene to elucidate its development.[103] Very recently, interesting topics like an emerging material system of graphene-based macroscopic assemblies and architectures, and the design and construction of 3D graphene-based composites for LIB applications have been introduced by different groups.[8,73,102,104] Graphene or graphene oxide can be also engineered into a sponge for energy-storage and environmental applications[70] owing to its high electrical conductivity, high specific surface area of 2600 m^2 g^{-1}, and larger number of active sites for lithium-ion storage and short lithium-ion diffusion pathway.[105]

Taking the above-mentioned advantages of graphene, we demonstrated the deposition of nanostructured MoO_2 or Fe_2O_3 on reduced graphene oxide to achieve excellent lithium-ion storage.[106] These are regarded as the most efficient ways to obtain graphene-based heterostructures. This type of heterostructure offers feasibility and good electrochemical performance over the single counterpart through the combination or reinforcement of each other. However, such materials will also suffer from some obvious drawbacks: i) the added active materials are partially exposed to the electrolyte, rendering their dissolution into the electrolyte during cycling; ii) the formation of an SEI on the surface of the nanoparticles with an unstable feature, leading to capacity fading; iii) the stacked electrode materials are not able to accommodate a large volume change and release the strain. To date, the development of more-efficient graphene-based anodes is still a big challenge. Recently, in order to solve the above problem, the 3D architecture of silicon nanoparticles encapsulated within a graphene shell, anchored on vertically aligned graphene trees[107] was developed as an advanced anode material for boosting LIBs (**Figure 8**). In this case, graphene played different roles in enhancing the overall electrochemical performance. The graphene nanosheets served as adaptable sealed wraps to synergistically accommodate the volume change of the wrapped silicon nanoparticles. Furthermore, the "graphene trees" directly grown on the current collector act as supports for graphene-wrapped silicon nanoparticles, ensuring their dispersion uniformity and supplying 3D short diffusion distances for both lithium-ion and electrons. A similar heterostructure of novel 3D porous graphene networks anchored with small and uniform Sn nanoparticles (5–30 nm)

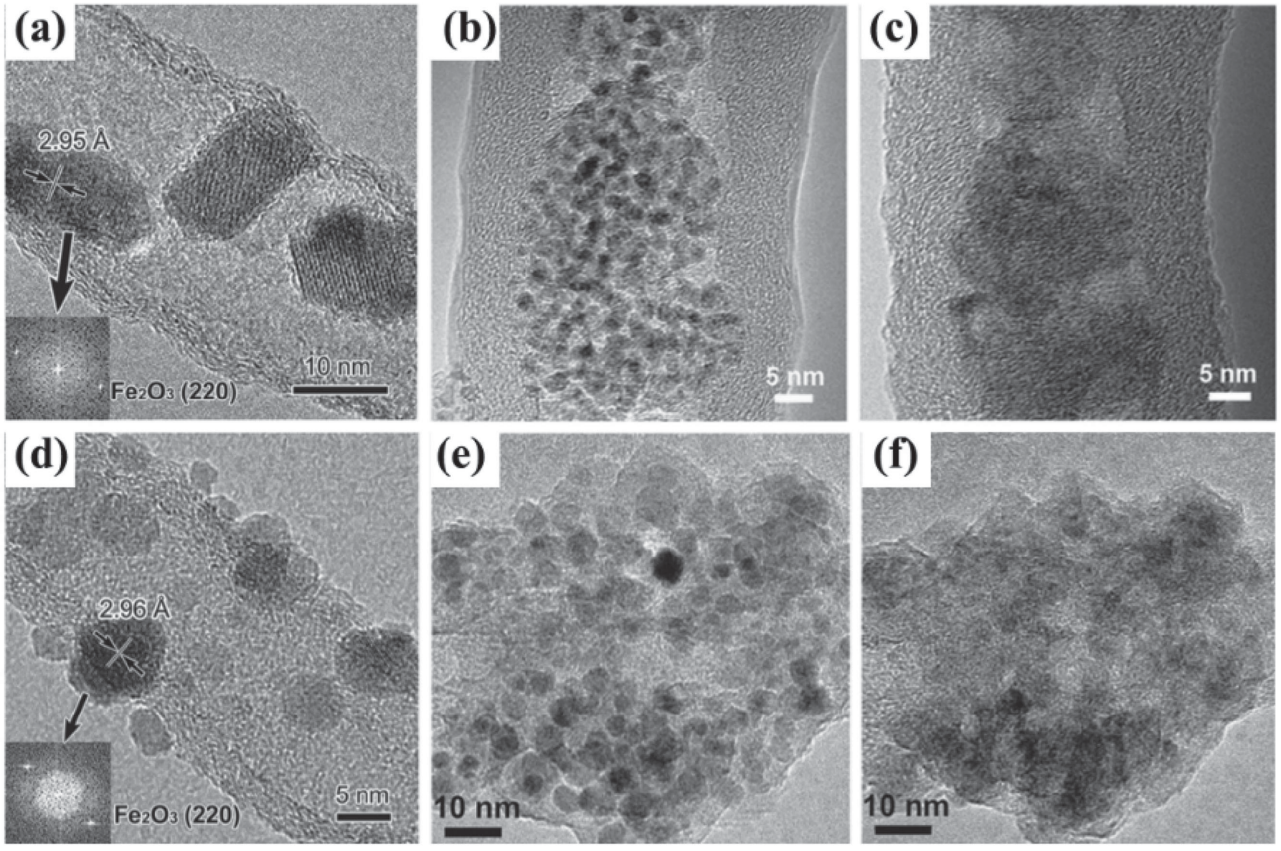

Figure 7. a–c) TEM images of the original prelithiated Fe_2O_3 nanoparticles confined in a CNT (a), and their structural change after the 1st charge (b) and the 1st discharge (c). d–f) Original Fe_2O_3 nanoparticles anchored on a CNT (d), and the corresponding structural change after the 1st charge (e) and the 1st discharge (f). Adapted with permission.[99] Copyright 2015, John Wiley & Sons, Inc.

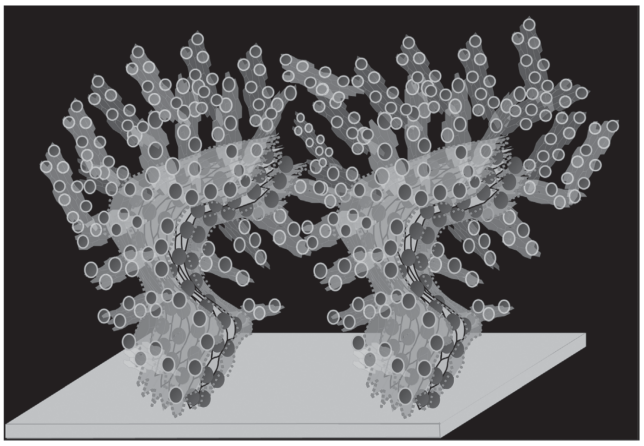

Figure 8. A graphic model of silicon nanoparticles encapsulated within a graphene shell anchored on 3D graphene trees. Reproduced with permission.[107] Copyright 2015, Elsevier.

encapsulated with graphene shells (ca. 1 nm) were also successfully fabricated by a facile and scalable one-step in situ CVD method.[108]

4.1.4. Carbon Coatings

With expectations of increasing the electrical conductivity and accommodating the volume change, carbon coatings or films have been rationally synthesized on various nanostructures to improve the lithium-storage performance of metal oxides or metal sulfides.[109–115] Moreover, a thin carbon layer can prevent the aggregation of metallic products during repeated electrochemical-conversion processes by acting as a barrier. To date, many synthetic strategies, such as CVD,[112] pyrolysis of carbon materials,[115] derivation of organic molecules,[75,116] polymer assisted deposition,[54,117] etc. have been applied for the preparation of thin carbon films on anode materials. Nanostructured α-Fe_2O_3 coated with a carbon layer with a thickness of around 3 nm (**Figure 9**a) was prepared via a simple pyrolysis of ferrocene.[111] A high reversible discharge capacity of 1138 mA h g^{-1} can be maintained even after 300 cycles at 500 mA g^{-1}. The heterostructured materials are able to deliver 458 mA h g^{-1} even when they are exposed to a high current density of 10 000 mA g^{-1}. Corresponding composition and structural studies revealed that the carbon layer grew with cycling, which was the main contributor to the high and ultra-stable LIB performance. Gao and co-workers also reported Fe_3O_4 nanoparticles with a carbon coating (Figure 9b) by CVD in C_2H_2 and Ar gas.[112] The thickness and content of the carbon layer can be readily controlled by tuning the deposition time (e.g., 2–3 nm for 10 min; 15–20 nm for 20 min). The most stable LIB performance was achieved for Fe_3O_4 with a carbon-coating thickness of 15–20 nm, which may be ascribed to the synergetic roles of increased conductivity, accommodated volume expansion, and buffered particle aggregation. Porous Fe_3O_4 microspheres (Figure 9c),[113] Fe_2O_3 rods (Figure 9d),[114] and MoO_2 nanoparticles (Figure 9e),[115] etc. with a carbon coating were successfully fabricated for LIBs with significantly enhanced electrochemical properties, in comparison to their single counterparts. However, the nature of a firmly combined interface between the carbon layer and the metal oxides or sulfides would consequently bring the risk of being cracked during the conversion reactions due to large

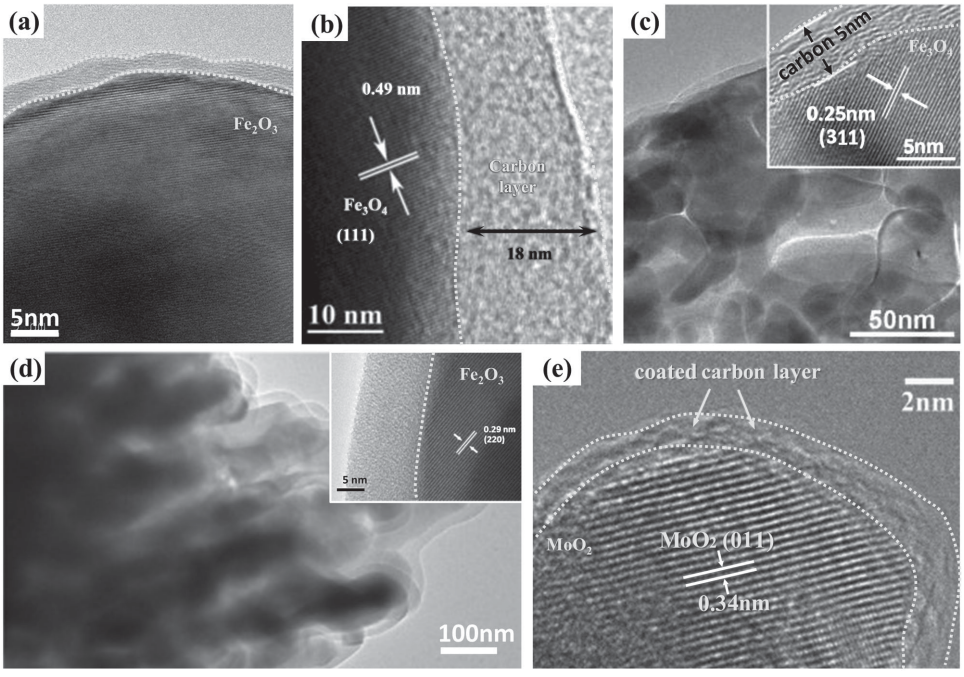

Figure 9. a–e) Carbon coatings on various transition metal oxides: Fe_2O_3 nanoparticles (a), Fe_3O_4 porous microspheres (b), Fe_2O_3 nanoarray (c), Fe_2O_3 rods (d), and MoO_2 nanoparticles (e), as anode materials for LIBs. Adapted with permission: Fe_2O_3 nanoparticles: ref. [111], Copyright 2015 and Fe_2O_3 microspheres: ref. [113], Copyright 2015, Royal Chemical Society; Fe_3O_4 nanoparticles: ref. [112], Copyright 2015, Fe_2O_3 nanorods: ref. [114], and MoO_2 nanoparticles: ref. [115], Copyright 2015, Elsevier.

volume change of the core, which is similar to the case of a lithium electrode with a carbon shell.[118] Another weakness of the transition-metal oxide–carbon core@shell system for LIBs is that the SEI layer is subject to continuous growth to cover the newly formed surface, due to pulverization of cores and the cracking of the old SEI layer, with the result of further impedance increase and capacity degradation.

Overall, carbon-supported heterostructures with robust structural integrity have been demonstrated, even subject to long cycling and high charge and discharge current densities. The performance enhancement of LIBs, using carbon-based heterostructures, was recently found to be caused by the change of SEI formation behavior, in which: i) it forms on the surface of the carbon instead of that of the encapsulated nanoparticles; ii) without repeated cracking and formation processes, the thickness of the SEI layer is reduced and more uniform. Kim and co-workers investigated the SEI-layer formation behavior of SnCo nanoparticles encapsulated into carbon nanofibers during cycling.[119] An effective and homogeneous SEI layer with a thickness of 86 nm was obtained after 100 cycles (97.9% capacity retention). On the contrary, a much thicker and continuously growing SEI layer (593 nm) was found for SnCo nanoparticles decorated on carbon nanofibers (71.9% capacity retention). This phenomenon has been further confirmed by studying the LIB of silicon particles encapsulated into graphene cages,[120] showing that a stable SEI layer was formed on the graphene cage instead of the silicon, which could minimize the irreversible consumption of lithium ions and increase the Coulombic efficiency in the early cycles.

4.2. Conducting-Polymer-Coated Electrode Materials

Conducting polymers are featured with good conductivity through a conjugated bond system along the polymer backbone.[121] In general principle, conducting polymers are formed either through chemical oxidation or electrochemical oxidation of the monomer.[122] Conducting polymers have continuously attracted research interest and attention since their discovery in 1976.[123] Due to their light weight, large capacitance, good electrical conductivity, ease of synthesis, and low cost, conducting polymers have become increasingly important as electrode materials over the recent few years.[121,122,124–126] However, flexible conducting polymers may be a double-edged sword when used independently as electrode materials because of the resulting poor stability during the charge/discharge process. Inspired by nature, the use of a conductive polymer as a skin or coating on a nanostructured anode material to form a frog-egg-like heterostructure for energy storage would provide it with combined advantages. The most commonly used conducting polymers include polyaniline (PANI), polypyrrole (PPy), poly(3,4-ethylenedioxythiophene) (PEDOT), and their derivatives.[122,125–129]

Researchers in the energy-storage field have constantly drawn inspiration from nature and continuously brought conceptual creative materials design and engineering into vision. Synthetic self-healing polymers, able to repair themselves and recover their functionalities despite being subjected to mechanical damage, have been proposed by Bao's group to stabilize silicon-microparticle anodes in LIBs.[130] A similar dilemma of mechanical cracks and fractures associated with the huge volume and structural change by the lithium insertion/extraction over the cycling process has been experimentally determined on various anode materials, making self-healing particularly desirable for energy storage. Conducting polymers with excellent stretchability and spontaneous self-healing capability may be a promising solution to alleviate the fast decay of electrode materials by reducing structural degradation and damage. By applying a conducting polymer in the preparation of electrode materials, no non-electroactive component, such as a binder and conductive carbon, is required for LIBs, which can greatly improve the active-material loadings, as well as the overall energy density. This is a so-called "all-in-one" highly integrated electrode. Kim and co-workers coated a very thin surface layer (contributing to less than 0.4 wt% of the total mass) on an electroactive material, $LiCoO_2$ (LCO) powder, by simply mixing LCO with an aqueous solution of poly(3,4-ethylenedioxythiophene) polystyrene sulfonate (PEDOT:PSS) (**Figure 10**).[131] The PEDOT skin layer, with a thickness of around 25 nm, on LCO works in a multifunctional way to provide electronic/ionic pathways and also bind LCO particles. The "all-in-one" electrode, with the highly conductive PEDOT:PSS coating, was shown to deliver higher volumetric capacities than its three-component (active material, conductive carbon, binder) counterpart. It is also noteworthy that it hinders the diffusion of LCO into the electrolyte, maintaining the integrity of the electrodes. Similar V_2O_5-nanoarray freestanding electrodes with a mesoporous thin layer of the conducting polymer (PEDOT) can be also obtained to compensate the common drawbacks of V_2O_5 by the two functions of polymer: good charge conductive path for the V_2O_5 nanoarray, as well as soft "armor" to protect the V_2O_5 core from pulverization.[125] The nanoscale engineering of electrode materials shares many similarities, and shows no fundamental differences between the cathodes and anodes. Based on such a concept, various conducting-polymer-based heterostructures, such as porous tremella-like MoS_2@PANI,[132] 3D a-Fe_2O_3@PPy,[126] vertically aligned MnO_2@PEDOT,[133] etc., have been developed as promising electrode materials for energy storage. However, the challenging issues associated with the application of a conducting polymer for LIBs can be the compromised stability of the SEI layer due to the soft nature of the conductive polymer, the conductive polymer being subject to dissolving into the electrolyte, a blocked ion-transport path caused by lithium ions trapped in the polymer, and other undesired side reactions introduced by the polymer.

4.3. Transition-Metal Compounds with Core@Shell Structure

Freestanding core/shell transition-metal compounds have sparked great interest for energy-storage applications due to their large surface areas, greater number of active surface sites, good ionic/electrical conductivity, and better permeability. Tremendous efforts have demonstrated that core–shell heterostructured electrode materials (Fe_2O_3@SnO_2, SnO_2@Mn_2O_3, Co_3O_4@Fe_2O_3, MnO@Mn_3N_2, SnO_2@WO_3, SnO_2@MoO_3, CuO@TiO_2, etc.[90,134–137]) could make use of the advantages of both components and offer better electrochemical properties

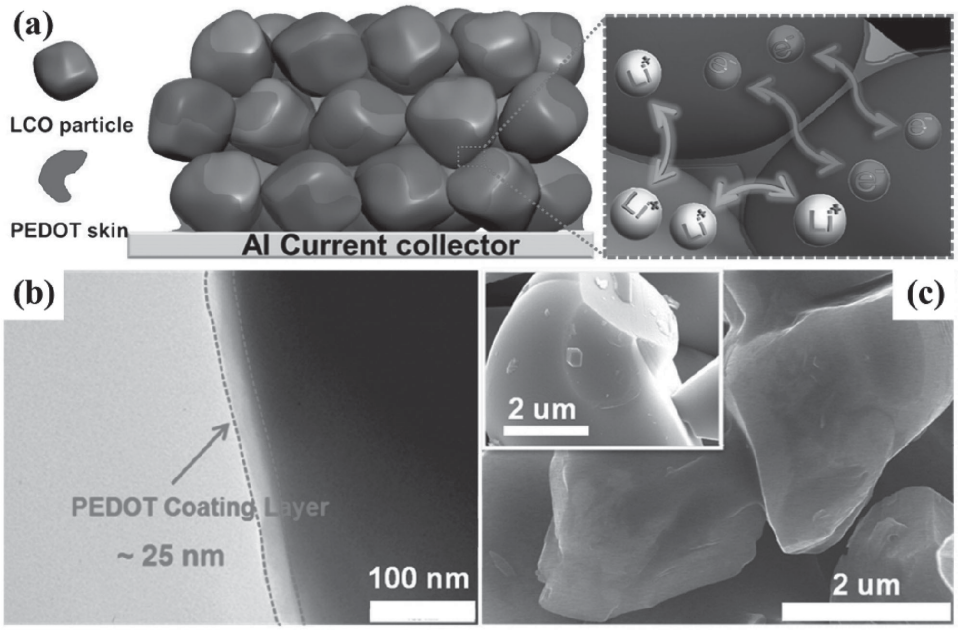

Figure 10. Structural and physicochemical identification of PEDOT:PSS skin layer on $LiCoO_2$ (LCO). a) Functions of PEDOT:PSS skin layer as an electrically, as well as an ionically conductive binder. b,c) TEM and SEM images of LCO@PEDOT:PSS. The inset in (c) shows SEM image of bare LCO. Reproduced with permission.[131] Copyright 2014, American Chemical Society.

over their single counterparts through a reinforcement or modification of each other.[138] Their high electrochemical activity is highly attributed to the complex chemical compositions and their synergetic effects, contributing to the exceptionally high specific capacity, which are typically several times higher than those of commercial graphite-/carbon-based electrode materials. Significantly, the interface/chemical distributions are homogeneous at the nanoscale; thus, a fast ion and electron transfer is guaranteed.[139] Moreover, they can provide a high surface area to increase the interfacial kinetics and porous texture to accommodate stress relaxation and a direct pathway for electron transport.[135,138,140] Fan and co-workers successfully prepared six-fold-symmetry branched α-Fe_2O_3@SnO_2 heterostructures (**Figure 11**) having Fe_2O_3 nanorods with a well-controlled length by the combination of CVD and a hydrothermal route.[136] Compared with the single component, the α-Fe_2O_3@SnO_2 heterostructure delivered enhanced performance as an anode in LIBs in terms of the low initial irreversible loss and the high reversible capacity due to the synergetic effect between the SnO_2 and the α-Fe_2O_3. The unique feature of the branched nanostructures also provides an increased specific surface area, ensuring the contact of the active material with the electrolyte. A similar α-MoO_3@MnO_2 core@shell heterostructure (**Figure 12**) was also fabricated by a facile two-step hydrothermal method with high discharge capacity (1475 mA h g^{-1} at 0.1 C), high rate capability (394 mA h g^{-1} at 6 C), and excellent cycling stability.[137] The well-defined core@shell structure of the nanorods was unambiguously recognized by TEM characterization and selected-area electron diffraction (SAED). Lithium ions and electrons were separately stored at the interfacial region, and lithium ions collected at the phase boundaries. Greater interfacial space between the MnO_2 nanowires and the α-MoO_3 nanorods could probably accommodate extra lithium ions.[141] Another interesting result is that ultrathin NiO nanosheets were grown uniformly on the porous $ZnCo_2O_4$ nanowires (ZCO@NiO) with many interparticle mesopores,[139] resulting in the formation of a 3D core@shell-nanowire-array heterostructure. The ZCO@NiO core@shell nanostructure exhibited significantly improved lithium-ion storage properties in terms of higher capacity, enhanced rate capability, and improved cycling stability compared with pristine $ZnCo_2O_4$ nanowire arrays. The superior lithium-storage performance of the ZCO@NiO nanowires can be attributed to their unique heterostructure. The merits of the synergetic effect from the two components, the enhanced electronic conductivity, and the interfacial lithium-storage potential from the heterostructured architecture, once again confirm the significance of the design and fabrication of novel heterostructured electrode materials for energy storage. However, their long-term stability for LIBs is still limited due to the possible large mismatch in volumetric expansion coefficient between the core and the shell during electrochemical cycling.

4.4. Combined Strategies to Novel Heterostructures

The combination of two or more strategies would necessarily adopt multiple favorable characteristics and push the output energy-storage capability to a high end. The insatiable appetite in conceptually novel heterostructures and the development of advanced synthetic strategies continuously drives the field forward. Increasing efforts have been devoted to the design and fabrication of combined conductive carbon or polymer with transition-metal compound heterostructures.[110,125,127,128,142] Graphene and CNTs can be engineered into a carbon scaffold or matrix for loading various anode materials. One typical

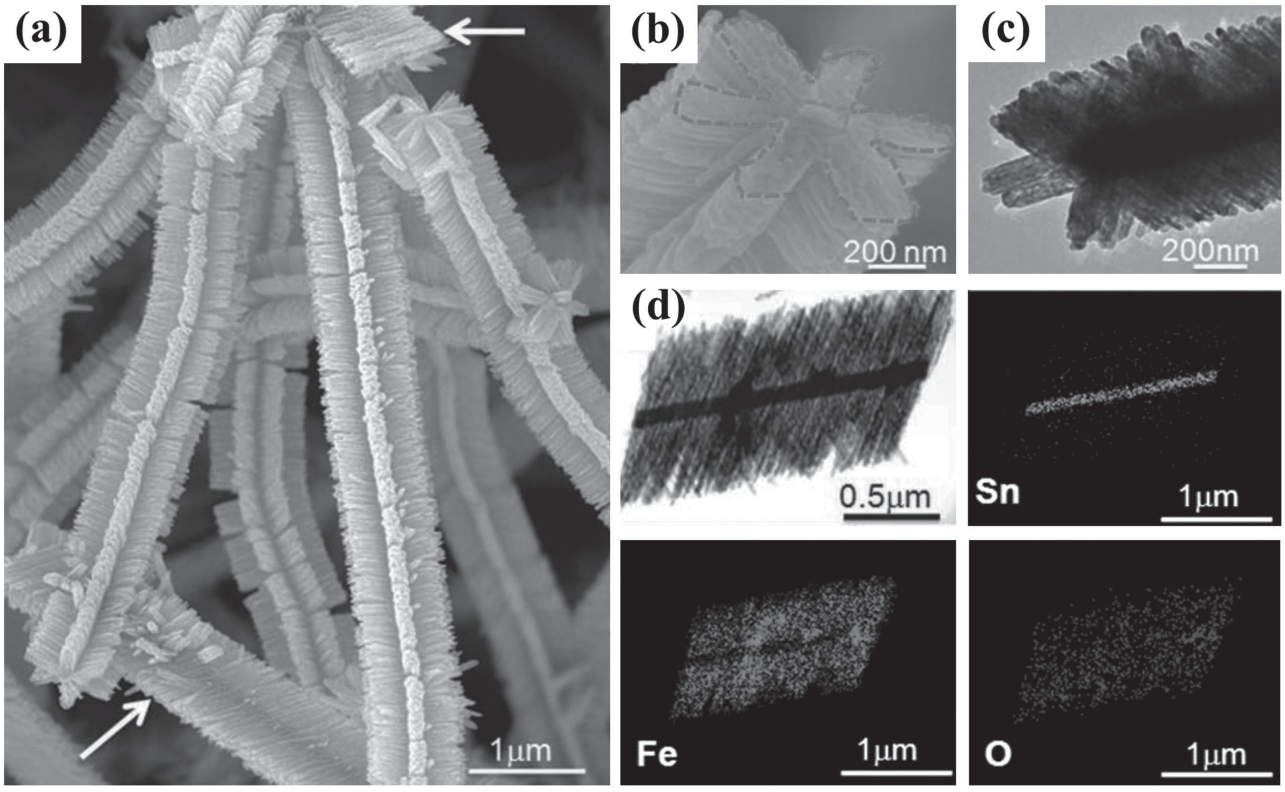

Figure 11. a–c) Typical SEM image (a) and high-magnification SEM and TEM images (b,c) of single six-fold-symmetry branched α-Fe_2O_3@SnO_2 heterostructures. d) TEM image of single branched nanowire and the corresponding elemental maps. Adapted with permission.[136] Copyright 2012, John Wiley & Sons, Inc.

example is that Fe_2O_3@SnO_2 nanoparticles decorated on graphene, with good flexibility, delivered an excellent high capacity of over 1000 mA h g^{-1} after 200 cycles,[143] ascribed to the synergistic effect of the Fe_2O_3 and the SnO_2, as well as the good electronic conductivity and rapid electrolyte diffusion path provided by the 3D interconnected porous graphene networks. Polymer-coated active materials, including transition-metal compounds with a complex architecture, can be combined with graphene sheets or CNTs, etc. A heterostructured composite of MnO_2/conjugated polymer/graphene displayed significantly enhanced battery performance because each component plays a favorable role in boosting LIBs.[127]

Flexible carbon-network-based electrode materials have been very attractive in recent years for EES applications because they offer unique flexibility for wearable devices. Various transition-metal compounds, e.g., titanium, nickel, cobalt, manganese or zinc oxides, hydroxides, or sulfides have been grown on carbon media, such as carbon cloth or carbon fiber.[87,144,145] Combining a transition-metal compound heterostructure and a flexible carbon network can offer interesting features for electrodes. 3D SnO_2@TiO_2 double-shell nanotubes on carbon cloth were recently fabricated as a flexible and binder-free anode with a long cycling life,[146] in which the SnO_2 pipe wall, with a thickness of 5 nm, can alleviate pulverization, and the TiO_2 layer plays a protective role. More recently, a novel synergistic TiO_2@MoO_3 core@shell-nanowire-array anode[147] was made by a facile hydrothermal method, followed by a subsequent controllable electrodeposition process. The TiO_2 arrays served as a stable scaffold and the MoO_3 provided large capacity (**Figure 13**). The loading mass of the MoO_3 can be well controlled by the electrode position, while the electrochemically stable TiO_2-nanowire core compensates the cycling instability of the MoO_3 shell. With an optimized mass ratio of TiO_2 to MoO_3 (1:1), the TiO_2@MoO_3 core@shell nanowire delivered high gravimetric capacity (670 mA h g^{-1}), excellent cyclability (>200 cycles) and good rate capability (up to 2000 mA g^{-1}). The strategy of engineering a synergistic core@shell-nanowire-array electrode on a flexible carbon substrate can be readily extended to other heterostructure designs, especially for electrode materials that are superior in capacity but inferior in cycling stability and rate performance. Nevertheless, the fabrication of flexible EES electrodes principally requires a flexible current collector, such as carbon cloth or fiber, bringing more challenges to the electrolyte and encapsulating materials.[144] Moreover, they deliver relatively low energy and power densities because of the limited mass loading, depending on their configuration nature. Experimental investigations are also required to confirm how robust the heterostructures will be when they are subject to repeated mechanical stretching or bending.

The nanoscale engineering of heterostructures offers such a wide variety of sceneries and opportunities. Taking the confined electrochemical reaction into consideration, we recently designed and prepared a robust yolk–shell nanospindles with sufficient internal void space for high-rate and long-term LIBs through a one-step in situ nanospace confined pyrolysis strategy (**Figure 14**a).[148] The particular hollow carbon nanospindles,

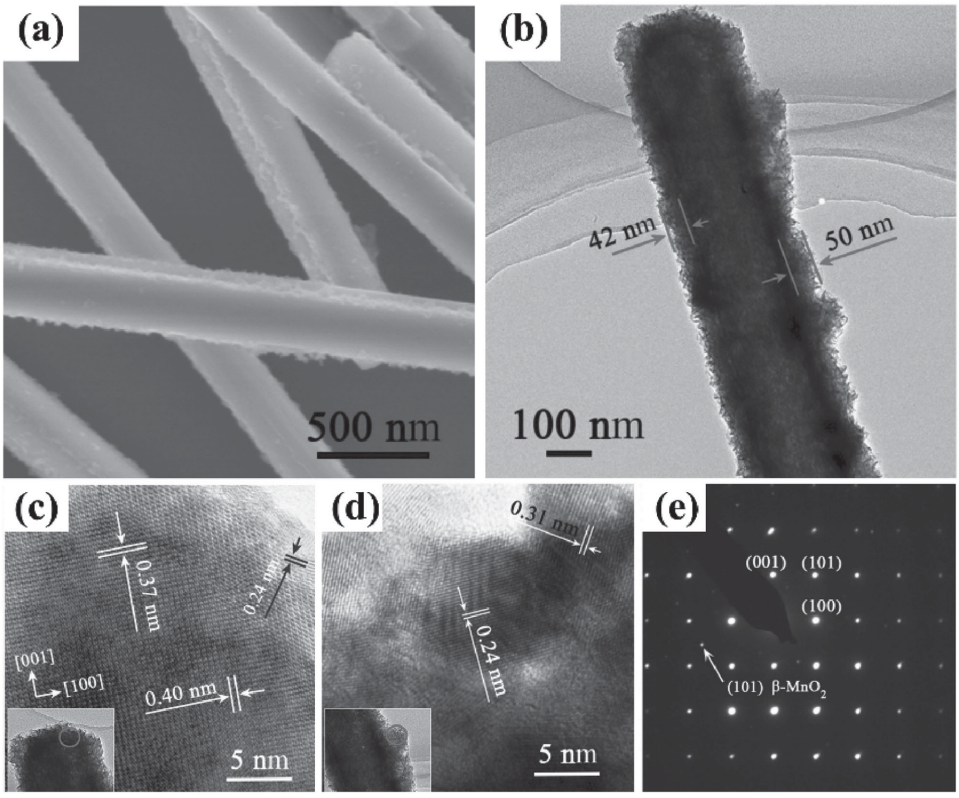

Figure 12. a) SEM image of α-MoO_3@MnO_2 core@shell heterostructure. b) TEM image of one single α-MoO_3@MnO_2 core@shell nanorod. c,d) HRTEM images at different selected regions. e) The SAED pattern taken for the nanorod. Adapted with permission.[137] Copyright 2014, Elsevier.

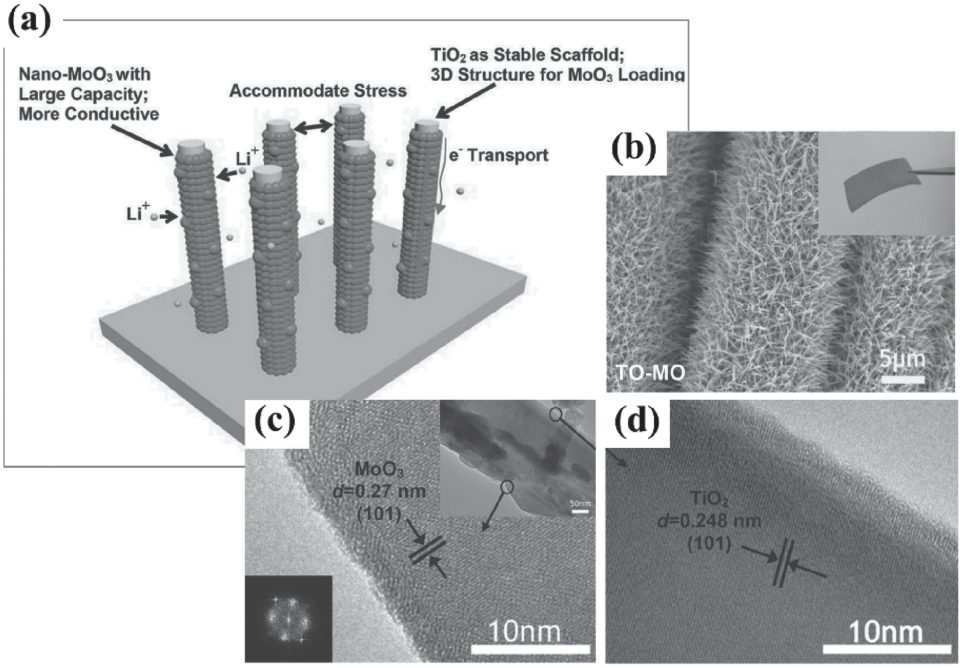

Figure 13. a) Schematic illustration of the structural features of the synergistic TiO_2@MoO_3 nanowire array. b) SEM images of the optimized TiO_2@MoO_3 hybrid array anode (inset in (b) is the optical image). c,d) High-resolution TEM images of MoO_3 nanoparticulate shell (c) and TiO_2 nanowire core (d) (inset: low-magnification picture of the optimized TiO_2@MoO_3 core@shell structure and FFT pattern of MoO_3). Adapted with permission.[147] Copyright 2015, American Chemical Society.

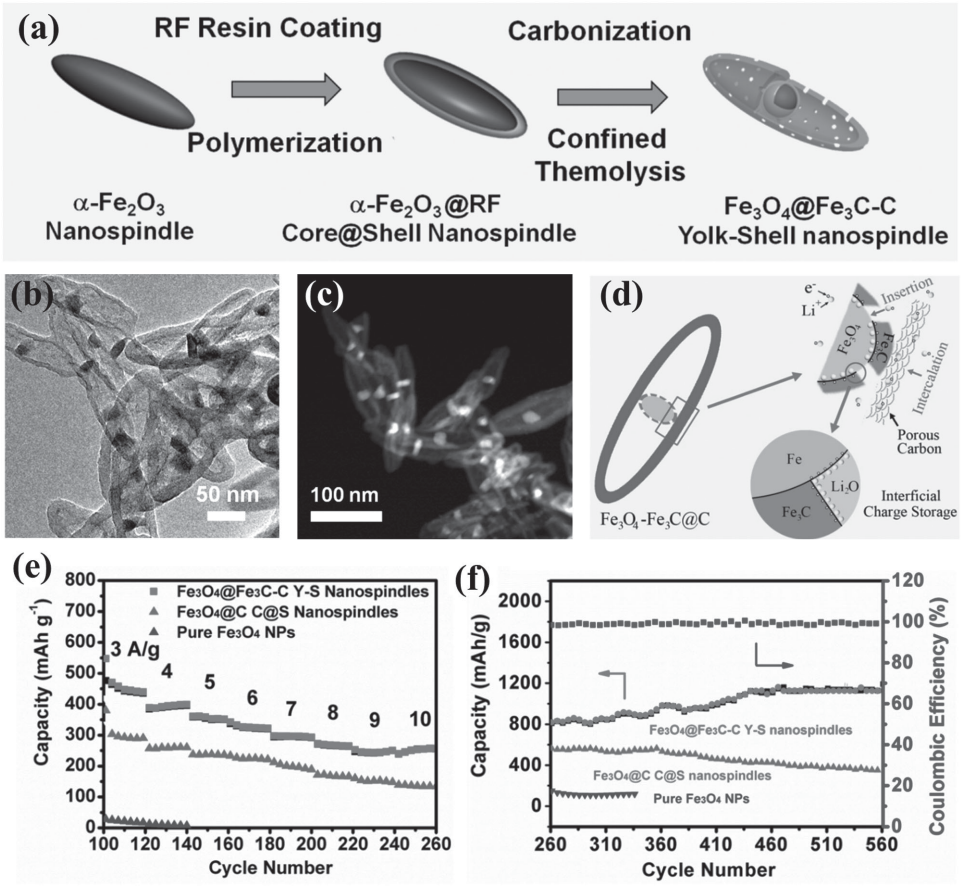

Figure 14. a) Schematic illustration on the synthesis of the Fe_3O_4@Fe_3C-C yolk–shell nanospindles. b–d) TEM image (b), STEM image (c), and proposed lithium storage by intercalation into the carbon pores and insertion into the lattice of active material, followed by additional charge separation at two-phase boundaries to form space charge layers (d). e) The capacity retention of Fe_3O_4@Fe_3C-C yolk–shell nanospindles, Fe_3O_4@C core@shell nanospindles, and pure Fe_3O_4 NPs from 500 to 2000 mA g^{-1}. f) Subsequent cycling tests at 500 mA g^{-1} from 261st to 560th cycle. Adapted and reproduced with permission.[148] Copyright 2015, American Chemical Society.

within which the Fe_3O_4@Fe_3C core@shell nanoparticle was well confined, (Figure 14b,c) offers desirable merits as electrode materials: the internal void space not only provides enough space for the expansion of the metal oxide inside, but also offers the double shell of the Fe_3C and carbon to hinder Fe_3O_4 dissolution (Figure 14d). No obvious change of the heterostructure was found after 660 cycles. As-obtained Fe_3O_4@Fe_3C-C yolk–shell nanospindles delivered a high reversible capacity, high rate capacity, and long-term cycling life (Figure 14e,f). They were superior to those of Fe_3O_4@C core@shell nanospindles and Fe_3O_4 nanoparticles and represented the most efficient Fe_3O_4-based anode material ever reported for LIBs. Compared with the previously discussed MnO@C NWs and silicon confined in CNTs, an Fe_3C layer was additionally introduced. The double shells strongly prevent the loss of active materials and maintain the excellent structural integrity. Meanwhile, the synergistic effect of the inorganic core@shell and porous carbon is responsible for the excellent electrochemical performance.

In addition to various core@shell anode materials, the nanoscale engineering of perforated structures to support active materials with high capacity is also highly promising. SnO_2–CNT composite microspheres[149] with a homogeneous distribution of interconnected pores were recently prepared by spray pyrolysis of a colloidal solution containing CNTs, tin oxalate, and polystyrene nanobeads. The obtained SnO_2–CNT composite microspheres provided a unique perforated structure (**Figure 15**), ensuring excellent lithium-storage properties as anode materials compared with either bare SnO_2 microspheres or SnO_2–CNT composite microspheres with filled spaces. The synergetic combination of interconnected pores and flexible CNTs effectively improves the electrochemical properties of SnO_2. The overall size on the micrometer scale, sufficient diffusion channels, and the intentionally created void space display combined advantages, such as high capacity, conductivity, and stability. The synthetic strategy can be easily extended for the preparation of other perforated metal-oxide–CNT composites by simply changing the precursor metal salts.

By applying multiple strategies, the tactful heterostructures and significantly enhanced LIB performances can be achieved. These complex heterostructures ensure the excellent electrochemical properties of the as-obtained anode materials by providing the combined merits of the above-mentioned strategies. Nonetheless, the procedures for preparing these heterostructures are also complicated, in which multiple steps are generally involved. The cost and complicated

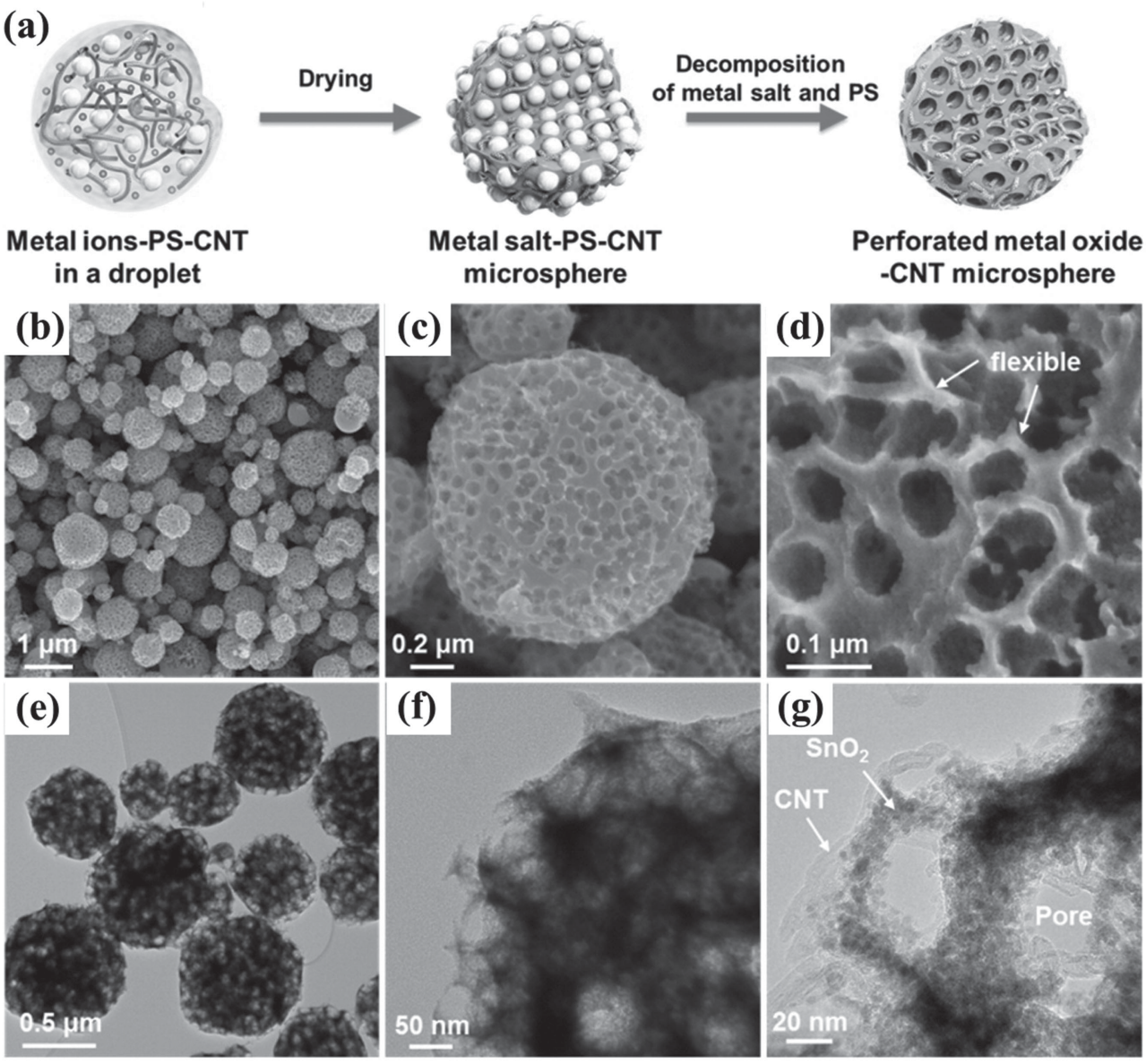

Figure 15. a) Schematic diagram of the formation of perforated SnO_2–CNT microspheres by one-step spray pyrolysis. b–g) The corresponding morphological and structural characterizations by SEM and TEM. Adapted with permission.[149] Copyright 2015, American Chemical Society.

synthetic process would pose a stumbling block to their practical applications.

5. Conclusions and Outlook

An update on the most recent advances in designing new heterostructured anode materials for boosting LIBs is presented. The typically selected cases are displayed in **Table 1**, including their synthetic method and electrochemical performances. Special emphasis is placed on the design and engineering of novel heterostructured anode materials with reduced size, large surface area, excellent electrical conductivity, structural stability, and fast electron and ion transport, which necessarily lead to remarkably enhanced LIB performances in terms of high capacity, long cycling lifespan, and durability at high rate. These heterostructures mainly take advantages of: i) supporting carbon materials with intrinsic high electronic conductivity, high surface area, and tunable porous structure; ii) conducting polymers featured with feasibility, light weight, large capacitance, good electric conductivity, ease of synthesis, and low cost; iii) special core@shell transition-metal compounds with a synergistic effect from both components and offering better electrochemical properties over their single counterpart; iv) combined strategies with comprehensive favorable characteristics. Nevertheless, these strategies may at the same time suffer from certain drawbacks, which are also summarized in Table 1, bringing sophisticated challenges to researchers. The

Table 1. Summary of the synthetic methods, electrochemical performances of typical heterostructured anode materials.

Category of heterostructures		Typical electrode materials	Synthetic method	Electrochemical performance	Advantages	Disadvantages
Carbon-supported anode materials (Section 4.1)	Porous carbon (Section 4.1.1)	MoS_2/mesoporous carbon with layered structure[77]	Heat treatment of dopamine polymerized MoS_2 nanosheets	1023 mA h g^{-1} at 400 mA g^{-1} (500th) 943 mA h g^{-1} at 6400 mA g^{-1} Low-temperature stability	1. High electrical conductivity 2. Large-surface area 3. Tunable carbon structure 4. High capacity 5. Low cost	1. Low Coulombic efficiency 2. Multi-step synthetic route
		MnO@C with peapod-like structure[81]	Heat treatment of MnO nanowire@ polydopamine	1199 mA h g^{-1} at 500 mA g^{-1} (100th) 463 mA h g^{-1} at 5000 mA g^{-1}		
	Carbon nanotubes (Section 4.1.2)	NiO@CNTs[93]	Templated solution synthesis	1034 mA h g^{-1} at 800 mA g^{-1} (300th)		
		Silicon-nanoparticles-filled CNTs[94]	Chemical vapor deposition	1475 mA h g^{-1} at 100 mA g^{-1} (20th)		
		Co_3O_4@CNTs[95]	Nanocasting	614 mA h g^{-1} at 2000 mA g^{-1} 700 mA h g^{-1} at 100 mA g^{-1} (60th) 408 mA h g^{-1} at 5000 mA g^{-1}		
		Fe_2O_3 nanoparticles confined in CNTs[99]	Anodic aluminum oxide template assisted method	963 mA h g^{-1} at 50 mA g^{-1} (16th)		
	Graphene (Section 4.1.3)	Silicon nanoparticles within a graphene shell[107]	Chemical vapor deposition	1353 mA h g^{-1} at 150 mA g^{-1} (50th) 412 mA h g^{-1} at 8000 mA g^{-1}		
	Carbon coating (Section 4.1.4)	Carbon-coated Fe_3O_4 microspheres[113]	Hydrothermal	1100 mA h g^{-1} at 200 mA g^{-1} (50th) 850 mA h g^{-1} at 1000 mA g^{-1}		
		Porous Fe_2O_3 rods coated with carbon[114]	Hydrothermal	639 mA h g^{-1} at 500 mA g^{-1} (300th) 429 mA h g^{-1} at 5000 mA g^{-1}		
		Carbon-coated MoO_2[115]	Solvothermal method with calcination treatment	1113 mA h g^{-1} at 80 mA g^{-1} (60th)		
Conducting-polymer-coated electrode materials (Section 4.2)		V_2O_5@PEDOT[125] (cathode)	Hydrothermal and electro-deposition	265 mA h g^{-1} at 5C (500th) 115 mA h g^{-1} at 80C (1C = 300 mA g^{-1})	1. Stretchability and spontaneous self-healing capability 2. Good conductivity 3. Soft "armor" to protect inside core from pulverization 4. "All-in-one" architecture	1. Dissolution 2. Compromised cycling stability 3. Low tolerance at high current density
		Fe_2O_3@PPy[126]	Chemical polymerization	0.42 mA h cm^{-2} at 0.1 mA cm^{-2} (100th) 0.32 mAh cm^{-2} at 1.0 mA cm^{-2}		
		MoS_2@PANI[132]	Polymerization and hydrothermal	915 mA h g^{-1} at 1000 mA g^{-1} (200th) 369 mA h g^{-1} at 4000 mA g^{-1}		
Transition-metal compounds with core@shell structure (Section 4.3)		α-Fe_2O_3@SnO_2[136]	Hydrothermal	1167 mA h g^{-1} at 100 mA g^{-1} (1st)	1. More active surface sites 2. Synergetic effect 3. Interfacial lithium storage	1. Low Coulombic efficiency 2. Unstable SEI formation 3. Low cycling stability
		$ZnCo_2O_4$@NiO[139]	Solution synthesis	1116 mA h g^{-1} at 100 mA g^{-1} (1st)		
		α-MoO_3@MnO_2[141]	Solution synthesis	1114 mA h g^{-1} at 0.2C (50th) 663 mA h g^{-1} at 2C (1C = 1080 mA g^{-1})		

Table 1. Continued

Category of heterostructures		Typical electrode materials	Synthetic method	Electrochemical performance	Advantages	Disadvantages
Combined strategies (Section 4.4)	4.3+4.1.3	Fe_2O_3@SnO_2 nanoparticles decorated on graphene[143]	Thermal reduction	1015 mA h g^{-1} at 100 mA g^{-1} (200th) 535 mA h g^{-1} at 2000 mA g^{-1}	1. Excellent structure integrity 2. High conductivity 3. High capacity 4. Long lifespan	1. Complicated synthetic process 2. High cost
	4.3+4.1.1	Fe_3O_4@Fe_3C nanoparticle confined in hollow carbon nanospindles[148]	Nanospace-confined pyrolysis	1128 mA h g^{-1} at 500 mA g^{-1} (560th) 423 mA h g^{-1} at 2000 mA g^{-1}		
	4.1.1+4.1.2	SnO_2–CNT composite microspheres[149]	Spray pyrolysis	796 mA h g^{-1} at 4000 mA g^{-1} (1000th) 671 mA h g^{-1} at 13 000 mA g^{-1}		

combined strategies will be favorable to build heterostructured electrode materials because they offer great versatility and diversity. With concerns around the cost and complexity of the production process, further advanced heterostructures are expected to emerge constantly in the near future. Therefore, the concept of materials engineering and design at the nanoscale is exceptionally important and plays an increasingly positive role in the development of electrode materials with high energy and power densities and good stability, as well as other features such as light weight, flexibility, etc. As demonstrated here, nanoscale engineering brings new visions into the fabrication of novel electrode materials, which can guarantee electrochemical performance, such as high energy and power density, and long lifespan. Well-controlled heterostructured electrode materials bring opportunities for the introduction and development of a full electric vehicle as the main form of ground transport. Moreover, other promising characteristics, such as flexibility, freestanding "all-in-one" architecture, and confined electrochemical reaction space, give these electrode materials the chance to paint a portrait on a much larger canvas.

Despite the great efforts, further considerations over heterostructured anode materials should be taken before stepping into practical applications:

i) Every goal, every endeavor, and every important achievement has to be built on basic science. The engineering and design of heterostructured electrode materials may involve crossing and multiple disciplinary skills, and experience in materials science, chemical engineering, physics, computational chemistry, electrochemistry, solid-state chemistry, etc. Only in this way, can the general principles be developed and applied for the future fabrication of complicated heterostructures.
ii) These LIB applications are only practical on the basis of low-cost, large-scale production, bringing more challenges to the synthetic strategies developed initially for lab-scale investigations.
iii) Insightful understanding of the mechanism on how the heterostructures improve the overall device performances. Powerful and advanced techniques such as micro-/nanoelectrodes and scanning electrochemical cell microscopy can expand our scope to the microscale, which may provide strong and direct evidence through in situ monitoring of the electrochemical process at the target position with considerable spatial resolution, and thus benefit the rational design of heterostructured anode materials with optimized device properties.
iv) General safety issues will be also brought to the surface with the utilization of new materials: how to optimize the heterostructures to minimize the effect of volume change and subsequent battery failure; how to deal with the environmental threat and recycling of new materials; how they work at harsh conditions with unyielding performance and safety.

The research on novel anode materials is very interesting and important. With rapid development in materials design and engineering at the nanoscale, we believe that heterostructured anode materials will lead to a bright future for boosting LIBs.

Acknowledgements

G.C. greatly acknowledges a 2015 ECS Edward G. Weston Summer Fellowship and Chinese Government Award for Outstanding Self-Financed Students Abroad from the China Scholarship Council. H.L. acknowledges partial funding support from the National Science Foundation DMR-1449035, the New Mexico EPSCoR with NSF-1301346, and Argonne National Laboratory. Argonne, a U.S. Department of Energy Office of Science laboratory, is operated under Contract No. DE-AC02-06CH11357. S.G. acknowledges financial support from the start-up funding of Peking University, National Key Research Program (SQ2016ZY02001813) and the Young Thousand Talented Program.

Received: January 11, 2016
Revised: March 27, 2016
Published online: June 15, 2016

[1] a) S. Chu, A. Majumdar, *Nature* **2012**, *488*, 294; b) G. P. Peters, G. Marland, C. Le Quere, T. Boden, J. G. Canadell, M. R. Raupach, *Nat. Clim. Change* **2012**, *2*, 2.
[2] a) H. D. Yoo, E. Markevich, G. Salitra, D. Sharon, D. Aurbach, *Mater. Today* **2014**, *17*, 110; b) K. Amine, R. Kanno, Y. Tzeng, *MRS Bull.* **2014**, *39*, 395; c) N.-S. Choi, Z. Chen, S. A. Freunberger, X. Ji, Y.-K. Sun, K. Amine, G. Yushin, L. F. Nazar, J. Cho, P. G. Bruce, *Angew. Chem. Int. Ed.* **2012**, *51*, 9994.
[3] J. Speirs, M. Contestabile, Y. Houari, R. Gross, *Renewable Sustainable Energy Rev.* **2014**, *35*, 183.

[4] *U.S. Department of Energy, Office of Energy Efficiency and Renewable Energy, About EV Everywhere*, http://energy.gov/eere/eveverywhere/about-ev-everywhere; accessed: August 2015.
[5] a) X. Su, Q. Wu, J. Li, X. Xiao, A. Lott, W. Lu, B. W. Sheldon, J. Wu, *Adv. Energy Mater.* **2014**, *4*, 1300882; b) J. R. Szczech, S. Jin, *Energy Environ. Sci.* **2011**, *4*, 56.
[6] a) C. Tan, H. Zhang, *Chem. Soc. Rev.* **2015**, *44*, 2713; b) S. Dong, X. Chen, X. Zhang, G. Cui, *Coord. Chem. Rev.* **2013**, *257*, 1946; c) V. Augustyn, P. Simon, B. Dunn, *Energy Environ. Sci.* **2014**, *7*, 1597; d) C. Yuan, H. B. Wu, Y. Xie, X. W. Lou, *Angew. Chem. Int. Ed.* **2014**, *53*, 1488.
[7] H. Wang, H. Yuan, S. Sae Hong, Y. Li, Y. Cui, *Chem. Soc. Rev.* **2015**, *44*, 2664.
[8] B. Luo, L. Zhi, *Energy Environ. Sci.* **2015**, *8*, 456.
[9] S. Han, D. Wu, S. Li, F. Zhang, X. Feng, *Adv. Mater.* **2014**, *26*, 849.
[10] B. Zhang, F. Kang, J.-M. Tarascon, J.-K. Kim, *Prog. Mater. Sci.* **2016**, *76*, 319.
[11] a) M.-R. Gao, Y.-F. Xu, J. Jiang, S.-H. Yu, *Chem. Soc. Rev.* **2013**, *42*, 2986; b) K. Zhang, X. Han, Z. Hu, X. Zhang, Z. Tao, J. Chen, *Chem. Soc. Rev.* **2015**, *44*, 699; c) T. Stephenson, Z. Li, B. Olsen, D. Mitlin, *Energy Environ. Sci.* **2014**, *7*, 209.
[12] S. Goriparti, E. Miele, F. De Angelis, E. Di Fabrizio, R. P. Zaccaria, C. Capiglia, *J. Power Sources* **2014**, *257*, 421.
[13] P. Roy, S. K. Srivastava, *J. Mater. Chem. A* **2015**, *3*, 2454.
[14] P. G. Bruce, B. Scrosati, J.-M. Tarascon, *Angew. Chem. Int. Ed.* **2008**, *47*, 2930.
[15] J. B. Goodenough, *Energy Environ. Sci.* **2014**, *7*, 14.
[16] Y. Wang, H. Li, P. He, E. Hosono, H. Zhou, *Nanoscale* **2010**, *2*, 1294.
[17] F. A. Soto, Y. Ma, J. M. M. de la Hoz, J. M. Seminario, P. B. Balbuena, *Chem. Mater.* **2015**, *27*, 7990.
[18] a) J. B. Goodenough, K.-S. Park, *J. Am. Chem. Soc.* **2013**, *135*, 1167; b) V. A. Agubra, J. W. Fergus, *J. Power Sources* **2014**, *268*, 153; c) D. Aurbach, *J. Power Sources* **2000**, *89*, 206.
[19] J. Marcicki, A. T. Conlisk, G. Rizzoni, *J. Power Sources* **2014**, *251*, 157.
[20] Z. Li, J. Huang, B. Y. Liaw, V. Metzler, J. Zhang, *J. Power Sources* **2014**, *254*, 168.
[21] M. V. Reddy, G. V. Subba Rao, B. V. R. Chowdari, *Chem. Rev.* **2013**, *113*, 5364.
[22] a) M. Armstrong, C. O'Dwyer, W. Macklin, J. D. Holmes, *Nano Res.* **2014**, *7*, 1; b) A. S. Arico, P. Bruce, B. Scrosati, J.-M. Tarascon, W. van Schalkwijk, *Nat. Mater.* **2005**, *4*, 366; c) L. Ji, Z. Lin, M. Alcoutlabi, X. Zhang, *Energy Environ. Sci.* **2011**, *4*, 2682.
[23] Z. Wang, L. Zhou, X. W. Lou, *Adv. Mater.* **2012**, *24*, 1903.
[24] S. L. Candelaria, Y. Shao, W. Zhou, X. Li, J. Xiao, J.-G. Zhang, Y. Wang, J. Liu, J. Li, G. Cao, *Nano Energy* **2012**, *1*, 195.
[25] Q. Zhang, E. Uchaker, S. L. Candelaria, G. Cao, *Chem. Soc. Rev.* **2013**, *42*, 3127.
[26] L. Fei, Y. Xu, X. Wu, Y. Li, P. Xie, S. Deng, S. Smirnov, H. Luo, *Nanoscale* **2013**, *5*, 11102.
[27] Y.-G. Guo, J.-S. Hu, L.-J. Wan, *Adv. Mater.* **2008**, *20*, 2878.
[28] Y.-M. Lin, P. R. Abel, A. Heller, C. B. Mullins, *J. Phys. Chem. Lett.* **2011**, *2*, 2885.
[29] C. K. Chan, H. Peng, G. Liu, K. McIlwrath, X. F. Zhang, R. A. Huggins, Y. Cui, *Nat. Nanotechnol.* **2008**, *3*, 31.
[30] D. Su, M. Ford, G. Wang, *Sci. Rep.* **2012**, *2*, 924.
[31] Z. Wu, B. Li, Y. Xue, J. Li, Y. Zhang, F. Gao, *J. Mater. Chem. A* **2015**, *3*, 19445.
[32] B. Li, J. Feng, Y. Qian, S. Xiong, *J. Mater. Chem. A* **2015**, *3*, 10336.
[33] D. D. Vaughn, O. D. Hentz, S. Chen, D. Wang, R. E. Schaak, *Chem. Commun.* **2012**, *48*, 5608.
[34] X. Gao, G. Li, Y. Xu, Z. Hong, C. Liang, Z. Lin, *Angew. Chem. Int. Ed.* **2015**, *54*, 14331.
[35] D. Li, C. Feng, H. K. Liu, Z. Guo, *Sci. Rep.* **2015**, *5*, 11326.
[36] Z. Wang, D. Luan, F. Y. C. Boey, X. W. Lou, *J. Am. Chem. Soc.* **2011**, *133*, 4738.
[37] X. W. Lou, C. Yuan, L. A. Archer, *Adv. Mater.* **2007**, *19*, 3328.
[38] Z. Wang, X. W. Lou, *Adv. Mater.* **2012**, *24*, 4124.
[39] X. Yao, C. Tang, G. Yuan, P. Cui, X. Xu, Z. Liu, *Electrochem. Commun.* **2011**, *13*, 1439.
[40] A. Keilbach, J. Moses, R. Köhn, M. Döblinger, T. Bein, *Chem. Mater.* **2010**, *22*, 5430.
[41] D. Y. Jiang, J. X. Zhao, M. Zhao, Q. C. Liang, S. Gao, J. M. Qin, Y. J. Zhao, A. Li, *J Alloys Compd.* **2012**, *532*, 31.
[42] A. L. Viet, M. V. Reddy, R. Jose, B. V. R. Chowdari, S. Ramakrishna, *J. Phys. Chem. C* **2010**, *114*, 664.
[43] J. Benson, S. Boukhalfa, A. Magasinski, A. Kvit, G. Yushin, *ACS Nano* **2012**, *6*, 118.
[44] Z. Xiao, Y. Xia, Z. Ren, Z. Liu, G. Xu, C. Chao, X. Li, G. Shen, G. Han, *J. Mater. Chem.* **2012**, *22*, 20566.
[45] X. Yao, X. Xin, Y. Zhang, J. Wang, Z. Liu, X. Xu, *J Alloys Compd.* **2012**, *521*, 95.
[46] P. Meduri, E. Clark, J. H. Kim, E. Dayalan, G. U. Sumanasekera, M. K. Sunkara, *Nano Lett.* **2012**, *12*, 1784.
[47] W. Luo, X. Hu, Y. Sun, Y. Huang, *J. Mater. Chem.* **2012**, *22*, 8916.
[48] a) G. Chen, S. S. Liaw, B. Li, Y. Xu, M. Dunwell, S. Deng, H. Fan, H. Luo, *J. Power Sources* **2014**, *251*, 338; b) G. Chen, E. Fu, M. Zhou, Y. Xu, L. Fei, S. Deng, V. Chaitanya, Y. Wang, H. Luo, *J. Alloy. Compd.* **2013**, *578*, 349.
[49] L. Ma, W.-X. Chen, L.-M. Xu, X.-P. Zhou, B. Jin, *Ceram. Int.* **2012**, *38*, 229.
[50] a) W. Zhou, Z. Yin, Y. Du, X. Huang, Z. Zeng, Z. Fan, H. Liu, J. Wang, H. Zhang, *Small* **2013**, *9*, 140; b) K. Zhang, H.-J. Kim, X. Shi, J.-T. Lee, J.-M. Choi, M.-S. Song, J. H. Park, *Inorg. Chem.* **2013**, *52*, 9807; c) X. Rui, H. Tan, Q. Yan, *Nanoscale* **2014**, *6*, 9889; d) S. Ding, J. S. Chen, X. W. Lou, *Chem. – Eur. J.* **2011**, *17*, 13142.
[51] Y. Sun, X. Hu, W. Luo, Y. Huang, *J. Mater. Chem.* **2012**, *22*, 13826.
[52] X. Zhang, Y. Qian, Y. Zhu, K. Tang, *Nanoscale* **2014**, *6*, 1725.
[53] J. S. Chen, T. Zhu, X. H. Yang, H. G. Yang, X. W. Lou, *J. Am. Chem. Soc.* **2010**, *132*, 13162.
[54] Y. Xu, M. Dunwell, L. Fei, E. Fu, Q. Lin, B. Patterson, B. Yuan, S. Deng, P. Andersen, H. Luo, G. Zou, *ACS Appl. Mater. Interfaces* **2014**, *6*, 20408.
[55] Y. Tang, X. Rui, Y. Zhang, T. M. Lim, Z. Dong, H. H. Hng, X. Chen, Q. Yan, Z. Chen, *J. Mater. Chem. A* **2013**, *1*, 82.
[56] H. Sun, M. Ahmad, J. Zhu, *Electrochim. Acta* **2013**, *89*, 199.
[57] Y. Lu, X. Yao, J. Yin, G. Peng, P. Cui, X. Xu, *RSC Adv.* **2015**, *5*, 7938.
[58] Z. Wang, D. Luan, S. Madhavi, C. Ming Li, X. Wen Lou, *Chem. Commun.* **2011**, *47*, 8061.
[59] X. W. Lou, Y. Wang, C. Yuan, J. Y. Lee, L. A. Archer, *Adv. Mater.* **2006**, *18*, 2325.
[60] S. Ding, J. S. Chen, G. Qi, X. Duan, Z. Wang, E. P. Giannelis, L. A. Archer, X. W. Lou, *J. Am. Chem. Soc.* **2011**, *133*, 21.
[61] X. W. Lou, D. Deng, J. Y. Lee, J. Feng, L. A. Archer, *Adv. Mater.* **2008**, *20*, 258.
[62] a) W. I. Park, C.-H. Lee, J. M. Lee, N.-J. Kim, G.-C. Yi, *Nanoscale* **2011**, *3*, 3522; b) L. Li, Z. Wu, S. Yuan, X.-B. Zhang, *Energy Environ. Sci.* **2014**, *7*, 2101; c) B. L. Ellis, P. Knauth, T. Djenizian, *Adv. Mater.* **2014**, *26*, 3368; d) H. Li, Z. Wang, L. Chen, X. Huang, *Adv. Mater.* **2009**, *21*, 4593; e) A. L. M. Reddy, S. R. Gowda, M. M. Shaijumon, P. M. Ajayan, *Adv. Mater.* **2012**, *24*, 5045.
[63] a) L. M. Jin, Y. C. Qiu, H. Deng, W. S. Li, H. Li, S. H. Yang, *Electrochim. Acta* **2011**, *56*, 9127; b) M. Li, W. Xu, W. Wang, Y. Liu, B. Cui, X. Guo, *J. Power Sources* **2014**, *248*, 465.
[64] a) G. K. Pradhan, D. K. Padhi, K. M. Parida, *ACS Appl. Mater. Interfaces* **2013**, *5*, 9101; b) B. You, N. Li, H. Zhu, X. Zhu, J. Yang, *ChemSusChem* **2013**, *6*, 474.
[65] J. L. Cheng, B. Wang, H. L. L. Xin, C. Kim, F. D. Nie, X. D. Li, G. C. Yang, H. Huang, *J. Mater. Chem. A* **2014**, *2*, 2701.

[66] W.-M. Zhang, X.-L. Wu, J.-S. Hu, Y.-G. Guo, L.-J. Wan, *Adv. Funct. Mater.* **2008**, *18*, 3941.
[67] G.-L. Xu, Y.-F. Xu, H. Sun, F. Fu, X.-M. Zheng, L. Huang, J.-T. Li, S.-H. Yang, S.-G. Sun, *Chem. Commun.* **2012**, *48*, 8502.
[68] a) F.-S. Li, Y.-S. Wu, J. Chou, M. Winter, N.-L. Wu, *Adv. Mater.* **2015**, *27*, 130; b) Y. Yao, N. Liu, M. T. McDowell, M. Pasta, Y. Cui, *Energy Environ. Sci.* **2012**, *5*, 7927; c) S. R. Gowda, A. L. M. Reddy, M. M. Shaijumon, X. Zhan, L. Ci, P. M. Ajayan, *Nano Lett.* **2010**, *11*, 101.
[69] J. Jiang, Y. Li, J. Liu, X. Huang, C. Yuan, X. W. Lou, *Adv. Mater.* **2012**, *24*, 5166.
[70] V. Chabot, D. Higgins, A. Yu, X. Xiao, Z. Chen, J. Zhang, *Energy Environ. Sci.* **2014**, *7*, 1564.
[71] a) M. Sevilla, R. Mokaya, *Energy Environ. Sci.* **2014**, *7*, 1250; b) J. L. Xie, C. X. Guo, C. M. Li, *Energy Environ. Sci.* **2014**, *7*, 2559; c) S. Mao, G. Lu, J. Chen, *Nanoscale* **2015**, *7*, 6924; d) J. Zai, X. Qian, *RSC Adv.* **2015**, *5*, 8814; e) X. Zhang, H. Zhang, C. Li, K. Wang, X. Sun, Y. Ma, *RSC Adv.* **2014**, *4*, 45862.
[72] a) D. Jariwala, V. K. Sangwan, L. J. Lauhon, T. J. Marks, M. C. Hersam, *Chem. Soc. Rev.* **2013**, *42*, 2824; b) M.-M. Titirici, R. J. White, N. Brun, V. L. Budarin, D. S. Su, F. del Monte, J. H. Clark, M. J. MacLachlan, *Chem. Soc. Rev.* **2015**, *44*, 250.
[73] H. Chang, H. Wu, *Energy Environ. Sci.* **2013**, *6*, 3483.
[74] a) Z. Zhang, Z. Li, F. Hao, X. Wang, Q. Li, Y. Qi, R. Fan, L. Yin, *Adv. Funct. Mater.* **2014**, *24*, 2500; b) C. Zhao, L. Liu, H. Zhao, A. Krall, Z. Wen, J. Chen, P. Hurley, J. Jiang, Y. Li, *Nanoscale* **2014**, *6*, 882.
[75] D. Shao, D. Tang, Y. Mai, L. Zhang, *J. Mater. Chem. A* **2013**, *1*, 15068.
[76] W. Li, Z. Yang, Y. Jiang, Z. Yu, L. Gu, Y. Yu, *Carbon* **2014**, *78*, 455.
[77] H. Jiang, D. Ren, H. Wang, Y. Hu, S. Guo, H. Hu, L. Zhang, C. Li, *Adv. Mater.* **2015**, *27*, 3687.
[78] J. Zhou, J. Qin, X. Zhang, C. Shi, E. Liu, J. Li, N. Zhao, C. He, *ACS Nano* **2015**, *9*, 3837.
[79] X.-Y. Yu, H. Hu, Y. Wang, H. Chen, X. W. Lou, *Angew. Chem. Int. Ed.* **2015**, *54*, 7395.
[80] Y. Xu, L. Fei, E. Fu, B. Yuan, J. Hill, Y. Chen, S. Deng, P. Andersen, Y. Wang, H. Luo, *J. Power Sources* **2013**, *242*, 604.
[81] H. Jiang, Y. Hu, S. Guo, C. Yan, P. S. Lee, C. Li, *ACS Nano* **2014**, *8*, 6038.
[82] N. Liu, Z. Lu, J. Zhao, M. T. McDowell, H.-W. Lee, W. Zhao, Y. Cui, *Nat. Nanotechnol.* **2014**, *9*, 187.
[83] S. Iijima, *Nature* **1991**, *354*, 56.
[84] a) C. Lu, W.-w. Liu, H. Li, B. K. Tay, *Chem. Commun.* **2014**, *50*, 3338; b) G. Zhou, D.-W. Wang, P.-X. Hou, W. Li, N. Li, C. Liu, F. Li, H.-M. Cheng, *J. Mater. Chem.* **2012**, *22*, 17942.
[85] S. J. Ee, H. Pang, U. Mani, Q. Yan, S. L. Ting, P. Chen, *ChemPhysChem* **2014**, *15*, 2445.
[86] a) X. Wang, G. Li, Z. Chen, V. Augustyn, X. Ma, G. Wang, B. Dunn, Y. Lu, *Adv. Energy Mater.* **2011**, *1*, 1089; b) Z. Chen, D. Zhang, X. Wang, X. Jia, F. Wei, H. Li, Y. Lu, *Adv. Mater.* **2012**, *24*, 2030; c) Z. Chen, V. Augustyn, J. Wen, Y. Zhang, M. Shen, B. Dunn, Y. Lu, *Adv. Mater.* **2011**, *23*, 791.
[87] X. Jia, Z. Chen, A. Suwarnasarn, L. Rice, X. Wang, H. Sohn, Q. Zhang, B. M. Wu, F. Wei, Y. Lu, *Energy Environ. Sci.* **2012**, *5*, 6845.
[88] L. Yan, Y. Xu, M. Zhou, G. Chen, S. Deng, S. Smirnov, H. Luo, G. Zou, *Electrochim. Acta* **2015**, *169*, 73.
[89] a) L. Sun, M. Li, Y. Jiang, W. Kong, K. Jiang, J. Wang, S. Fan, *Nano Lett.* **2014**, *14*, 4044; b) D. Ren, H. Jiang, Y. Hu, L. Zhang, C. Li, *RSC Adv.* **2014**, *4*, 40368; c) Y. Shi, Y. Wang, J. I. Wong, A. Y. S. Tan, C.-L. Hsu, L.-J. Li, Y.-C. Lu, H. Y. Yang, *Sci. Rep.* **2013**, *3*, 2169; d) Y. Yu, F. Pan, J. Wang, Z. Yang, L. Gu, *RSC Adv.* **2015**, *5*, 77518; e) S. Chen, P. Bao, G. Wang, *Nano Energy* **2013**, *2*, 425; f) Y. Zhong, X. Li, Y. Zhang, R. Li, M. Cai, X. Sun, *Appl. Surf. Sci.* **2015**, *332*, 192; g) X. Meng, S. C. Riha, J. A. Libera, Q. Wu, H.-H. Wang, A. B. F. Martinson, J. W. Elam, *J. Power Sources* **2015**, *280*, 621.
[90] Y. Fan, Q. Zhang, C. X. Lu, Q. Z. Xiao, X. H. Wang, B. K. Tay, *Nanoscale* **2013**, *5*, 1503.
[91] a) S. Nardecchia, D. Carriazo, M. L. Ferrer, M. C. Gutierrez, F. del Monte, *Chem. Soc. Rev.* **2013**, *42*, 794; b) H. Wang, H. Dai, *Chem. Soc. Rev.* **2013**, *42*, 3088; c) R. H. Baughman, A. A. Zakhidov, W. A. de Heer, *Science* **2002**, *297*, 787.
[92] H. Yoo, A. P. Tiwari, J. Lee, D. Kim, J. H. Park, H. Lee, *Nanoscale* **2015**, *7*, 3404.
[93] X. Xu, H. Tan, K. Xi, S. Ding, D. Yu, S. Cheng, G. Yang, X. Peng, A. Fakeeh, R. V. Kumar, *Carbon* **2015**, *84*, 491.
[94] W.-J. Yu, C. Liu, P.-X. Hou, L. Zhang, X.-Y. Shan, F. Li, H.-M. Cheng, *ACS Nano* **2015**, *9*, 5063.
[95] D. Gu, W. Li, F. Wang, H. Bongard, B. Spliethoff, W. Schmidt, C. Weidenthaler, Y. Xia, D. Zhao, F. Schüth, *Angew. Chem. Int. Ed.* **2015**, *54*, 7060.
[96] C.-j. Liu, H. Huang, G.-z. Cao, F.-h. Xue, R. A. P. Camacho, X.-l. Dong, *Electrochim. Acta* **2014**, *144*, 376.
[97] W.-J. Yu, P.-X. Hou, F. Li, C. Liu, *J. Mater. Chem.* **2012**, *22*, 13756.
[98] W. Chen, Z. Fan, L. Gu, X. Bao, C. Wang, *Chem. Commun.* **2010**, *46*, 3905.
[99] W.-J. Yu, L. Zhang, P.-X. Hou, F. Li, C. Liu, H.-M. Cheng, *Adv. Energy Mater.* **2015**, DOI: 10.1002/aenm.201501755.
[100] K. S. Novoselov, A. K. Geim, S. V. Morozov, D. Jiang, Y. Zhang, S. V. Dubonos, I. V. Grigorieva, A. A. Firsov, *Science* **2004**, *306*, 666.
[101] a) X. Huang, Z. Zeng, Z. Fan, J. Liu, H. Zhang, *Adv. Mater.* **2012**, *24*, 5979; b) Y. Sun, Q. Wu, G. Shi, *Energy Environ. Sci.* **2011**, *4*, 1113.
[102] C. Xu, B. Xu, Y. Gu, Z. Xiong, J. Sun, X. S. Zhao, *Energy Environ. Sci.* **2013**, *6*, 1388.
[103] K. S. Novoselov, V. I. Falko, L. Colombo, P. R. Gellert, M. G. Schwab, K. Kim, *Nature* **2012**, *490*, 192.
[104] a) H.-P. Cong, J.-F. Chen, S.-H. Yu, *Chem. Soc. Rev.* **2014**, *43*, 7295; b) X. Cao, Z. Yin, H. Zhang, *Energy Environ. Sci.* **2014**, *7*, 1850.
[105] F. Bonaccorso, L. Colombo, G. Yu, M. Stoller, V. Tozzini, A. C. Ferrari, R. S. Ruoff, V. Pellegrini, *Science* **2015**, *347*, 1246501.
[106] a) Y. Xu, R. Yi, B. Yuan, X. Wu, M. Dunwell, Q. Lin, L. Fei, S. Deng, P. Andersen, D. Wang, H. Luo, *J. Phys. Chem. Lett.* **2012**, *3*, 309; b) G. Chen, R. Rodriguez, L. Fei, Y. Xu, S. Deng, S. Smirnov, H. Luo, *J. Power Sources* **2014**, *259*, 227.
[107] N. Li, S. Jin, Q. Liao, H. Cui, C. X. Wang, *Nano Energy* **2014**, *5*, 105.
[108] J. Qin, C. He, N. Zhao, Z. Wang, C. Shi, E.-Z. Liu, J. Li, *ACS Nano* **2014**, *8*, 1728.
[109] a) Z. Zhang, L. Zhang, W. Li, A. Yu, P. Wu, *ACS Appl. Mater. Interfaces* **2015**, *7*, 10395; b) X. Jiang, X. Yang, Y. Zhu, Y. Yao, P. Zhao, C. Li, *J. Mater. Chem. A* **2015**, *3*, 2361; c) J. Qin, X. Zhang, N. Zhao, C. Shi, E.-Z. Liu, J. Li, C. He, *J. Mater. Chem. A* **2015**, *3*, 23170; d) G. Gao, H. B. Wu, S. Ding, X. W. Lou, *Small* **2015**, *11*, 432.
[110] H. Liu, Z. Li, Y. Liang, R. Fu, D. Wu, *Carbon* **2015**, *84*, 419.
[111] X. Lv, J. Deng, J. Wang, J. Zhong, X. Sun, *J. Mater. Chem. A* **2015**, *3*, 5183.
[112] J. Wang, M. Gao, D. Wang, X. Li, Y. Dou, Y. Liu, H. Pan, *J. Power Sources* **2015**, *282*, 257.
[113] Y. Wang, L. Zhang, Y. Wu, Y. Zhong, Y. Hu, X. W. Lou, *Chem. Commun.* **2015**, *51*, 6921.
[114] X. Cai, H. Lin, X. Zheng, X. Chen, P. Xia, X. Luo, X. Zhong, X. Li, W. Li, *Electrochim. Acta* **2016**, *191*, 767.
[115] Y. Zhou, Q. Liu, D. Liu, H. Xie, G. Wu, W. Huang, Y. Tian, Q. He, A. Khalil, Y. A. Haleem, T. Xiang, W. Chu, C. Zou, L. Song, *Electrochim. Acta* **2015**, *174*, 8.
[116] a) J. Li, Q. Ru, S. J. Hu, D. W. Sun, B. B. Zhang, X. H. Hou, *Electrochim. Acta* **2013**, *113*, 505; b) T. Zhu, J. S. Chen, X. W. Lou, *J. Phys. Chem. C* **2011**, *115*, 9814.

[117] a) Y. Jiang, G. Chen, X. Xu, X. Chen, S. Deng, S. Smirnov, H. Luo, G. Zou, *RSC Adv.* **2014**, *4*, 48938; b) Y. Xu, L. Fei, E. Fu, B. Yuan, J. Hill, Y. Chen, S. Deng, P. Andersen, Y. Wang, H. Luo, *J. Power Sources* **2013**, *242*, 604.
[118] G. Y. Zheng, S. W. Lee, Z. Liang, H. W. Lee, K. Yan, H. B. Yao, H. T. Wang, W. Y. Li, S. Chu, Y. Cui, *Nat. Nanotechnol.* **2014**, *9*, 618.
[119] J. Shin, W.-H. Ryu, K.-S. Park, I.-D. Kim, *ACS Nano* **2013**, *7*, 7330.
[120] Y. Li, K. Yan, H.-W. Lee, Z. Lu, N. Liu, Y. Cui, *Nat. Energy* **2016**, *1*, 15029.
[121] G. A. Snook, P. Kao, A. S. Best, *J. Power Sources* **2011**, *196*, 1.
[122] Y.-Z. Long, M.-M. Li, C. Gu, M. Wan, J.-L. Duvail, Z. Liu, Z. Fan, *Prog. Polym. Sci.* **2011**, *36*, 1415.
[123] H. Shirakawa, E. J. Louis, A. G. MacDiarmid, C. K. Chiang, A. J. Heeger, *J. Chem. Soc., Chem. Commun.* **1977**, 578.
[124] a) W. Wu, R. Tang, Q. Li, Z. Li, *Chem. Soc. Rev.* **2015**, *44*, 3997; b) L. Pan, G. Yu, D. Zhai, H. R. Lee, W. Zhao, N. Liu, H. Wang, B. C.-K. Tee, Y. Shi, Y. Cui, Z. Bao, *Proc. Natl. Acad. Sci. USA* **2012**, *109*, 9287; c) H. S. Oh, H. M. Jeong, J. H. Park, I.-W. Ock, J. K. Kang, *J. Mater. Chem. A* **2015**, *3*, 10238; d) J.-M. Jeong, B. G. Choi, S. C. Lee, K. G. Lee, S.-J. Chang, Y.-K. Han, Y. B. Lee, H. U. Lee, S. Kwon, G. Lee, C.-S. Lee, Y. S. Huh, *Adv. Mater.* **2013**, *25*, 6250; e) L. Yue, S. Q. Wang, X. Y. Zhao, L. Z. Zhang, *J. Mater. Chem.* **2012**, *22*, 1094; f) D. Ghosh, S. Giri, M. Mandal, C. K. Das, *RSC Adv.* **2014**, *4*, 26094; g) H. M. Liu, D. Saikia, H. C. Wu, C. Y. Su, T. H. Wang, Y. H. Li, J. P. Pan, H. M. Kao, *RSC Adv.* **2014**, *4*, 56147; h) K. Pal, V. Panwar, S. Bag, J. Manuel, J.-H. Ahn, J. K. Kim, *RSC Adv.* **2015**, *5*, 3005; i) W. Y. Li, Q. F. Zhang, G. Y. Zheng, Z. W. Seh, H. B. Yao, Y. Cui, *Nano Lett.* **2013**, *13*, 5534; j) H. Zhao, Z. H. Wang, P. Lu, M. Jiang, F. F. Shi, X. Y. Song, Z. Y. Zheng, X. Zhou, Y. B. Fu, G. Abdelbast, X. C. Xiao, Z. Liu, V. S. Battaglia, K. Zaghib, G. Liu, *Nano Lett.* **2014**, *14*, 6704; k) P. M. Dziewonski, M. Grzeszczuk, *Electrochim. Acta* **2010**, *55*, 3336; l) J. Chen, Y. Liu, A. I. Minett, C. Lynam, J. Z. Wang, G. G. Wallace, *Chem. Mater.* **2007**, *19*, 3595; m) J. C. Guo, C. S. Wang, *Chem. Commun.* **2010**, *46*, 1428; n) P. Li, Y. Yang, E. Shi, Q. Shen, Y. Shang, S. Wu, J. Wei, K. Wang, H. Zhu, Q. Yuan, A. Cao, D. Wu, *ACS Appl. Mater. Interfaces* **2014**, *6*, 5228; o) Y. Yang, G. Yu, J. J. Cha, H. Wu, M. Vosgueritchian, Y. Yao, Z. Bao, Y. Cui, *ACS Nano* **2011**, *5*, 9187.
[125] D. L. Chao, X. H. Xia, J. L. Liu, Z. X. Fan, C. F. Ng, J. Y. Lin, H. Zhang, Z. X. Shen, H. J. Fan, *Adv. Mater.* **2014**, *26*, 5794.
[126] J. L. Liu, W. W. Zhou, L. F. Lai, H. P. Yang, S. H. Lim, Y. D. Zhen, T. Yu, Z. X. Shen, J. Y. Lin, *Nano Energy* **2013**, *2*, 726.
[127] C. X. Guo, M. Wang, T. Chen, X. W. Lou, C. M. Li, *Adv. Energy Mater.* **2011**, *1*, 736.
[128] F. Han, D. Li, W. C. Li, C. Lei, Q. Sun, A. H. Lu, *Adv. Funct. Mater.* **2013**, *23*, 1692.
[129] a) H. M. Song, D. Y. Yoo, S. K. Hong, J. S. Kim, W. I. Cho, S. I. Mho, *Electroanalysis* **2011**, *23*, 2094; b) X. W. Gao, J. Z. Wang, S. L. Chou, H. K. Liu, *J. Power Sources* **2012**, *220*, 47; c) J. Duay, E. Gillette, R. Liu, S. B. Lee, *Phys. Chem. Chem. Phys.* **2012**, *14*, 3329.
[130] C. Wang, H. Wu, Z. Chen, M. T. McDowell, Y. Cui, Z. Bao, *Nat. Chem.* **2013**, *5*, 1042.
[131] J. M. Kim, H. S. Park, J. H. Park, T. H. Kim, H. K. Song, S. Y. Lee, *ACS Appl. Mater. Interfaces* **2014**, *6*, 12789.
[132] H. Liu, F. Zhang, W. Li, X. Zhang, C.-S. Lee, W. Wang, Y. Tang, *Electrochim. Acta* **2015**, *167*, 132.
[133] a) R. Liu, J. Duay, S. B. Lee, *ACS Nano* **2010**, *4*, 4299; b) R. Liu, S. B. Lee, *J. Am. Chem. Soc.* **2008**, *130*, 2942.
[134] a) Q. Wang, Q. Wang, D. A. Zhang, J. Sun, L. L. Xing, X. Y. Xue, *Chem. Asian J.* **2014**, *9*, 3299; b) Y. F. Li, Y. J. Hu, H. Jiang, X. Y. Hou, C. Z. Li, *CrystEngComm* **2013**, *15*, 6715; c) L. L. Xing, P. Deng, B. He, Y. X. Nie, X. L. Wu, S. Yuan, C. X. Cui, X. Y. Xue, *Electrochim. Acta* **2014**, *118*, 45; d) C. Chen, S. H. Lee, M. Cho, Y. Lee, *Mater. Lett.* **2015**, *140*, 111; e) S. Yuan, D.-l. Ma, S. Wang, Y. Liu, X. Yang, Z. Cao, *Mater. Lett.* **2015**, *145*, 104; f) J. S. Chen, C. M. Li, W. W. Zhou, Q. Y. Yan, L. A. Archer, X. W. Lou, *Nanoscale* **2009**, *1*, 280; g) Y. M. Wu, M. J. Liu, H. B. Feng, J. H. Li, *Nanoscale* **2014**, *6*, 14697; h) Y. S. Luo, D. Z. Kong, J. S. Luo, Y. L. Wang, D. Y. Zhang, K. W. Qiu, C. W. Cheng, C. M. Li, T. Yu, *RSC Adv.* **2014**, *4*, 13241; i) H. Wu, M. Xu, Y. Wang, G. Zheng, *Nano Res.* **2013**, *6*, 167; j) J. Cheng, Y. Lu, K. Qiu, H. Yan, J. Xu, L. Han, X. Liu, J. Luo, J.-K. Kim, Y. Luo, *Sci. Rep.* **2015**, *5*, 12099.
[135] a) X. Y. Xue, Z. H. Chen, L. L. Xing, S. Yuan, Y. J. Chen, *Chem. Commun.* **2011**, *47*, 5205; b) Y. S. Luo, J. S. Luo, J. Jiang, W. W. Zhou, H. P. Yang, X. Y. Qi, H. Zhang, H. J. Fan, D. Y. W. Yu, C. M. Li, T. Yu, *Energy Environ. Sci.* **2012**, *5*, 6559.
[136] W. Zhou, C. Cheng, J. Liu, Y. Y. Tay, J. Jiang, X. Jia, J. Zhang, H. Gong, H. H. Hng, T. Yu, H. J. Fan, *Adv. Funct. Mater.* **2011**, *21*, 2439.
[137] Q. Wang, D. A. Zhang, Q. Wang, J. Sun, L. L. Xing, X. Y. Xue, *Electrochim. Acta* **2014**, *146*, 411.
[138] X. Xia, J. Tu, Y. Zhang, X. Wang, C. Gu, X.-b. Zhao, H. J. Fan, *ACS Nano* **2012**, *6*, 5531.
[139] Z. P. Sun, W. Ai, J. L. Liu, X. Y. Qi, Y. L. Wang, J. H. Zhu, H. Zhang, T. Yu, *Nanoscale* **2014**, *6*, 6563.
[140] X. Lu, T. Zhai, X. Zhang, Y. Shen, L. Yuan, B. Hu, L. Gong, J. Chen, Y. Gao, J. Zhou, Y. Tong, Z. L. Wang, *Adv. Mater.* **2012**, *24*, 938.
[141] J. Maier, *Faraday Discuss.* **2007**, *134*, 51.
[142] a) G. Jeong, J. G. Kim, M. S. Park, M. Seo, S. M. Hwang, Y. U. Kim, Y. J. Kim, J. H. Kim, S. X. Dou, *ACS Nano* **2014**, *8*, 2977; b) L. Hu, Y. Ren, H. Yang, Q. Xu, *ACS Appl. Mater. Interfaces* **2014**, *6*, 14644.
[143] S. Liu, R. Wang, M. Liu, J. Luo, X. Jin, J. Sun, L. Gao, *J. Mater. Chem. A* **2014**, *2*, 4598.
[144] X. Wang, X. Lu, B. Liu, D. Chen, Y. Tong, G. Shen, *Adv. Mater.* **2014**, *26*, 4763.
[145] a) L. Noerochim, J.-Z. Wang, S.-L. Chou, D. Wexler, H.-K. Liu, *Carbon* **2012**, *50*, 1289; b) H. Gwon, J. Hong, H. Kim, D.-H. Seo, S. Jeon, K. Kang, *Energy Environ. Sci.* **2014**, *7*, 538; c) L. Bao, J. Zang, X. Li, *Nano Lett.* **2011**, *11*, 1215; d) S. Fang, L. Shen, P. Nie, G. Xu, L. Yang, H. Zheng, X. Zhang, *Part. Part. Syst. Charact.* **2015**, *32*, 364; e) T. Song, H. Han, H. Choi, J. W. Lee, H. Park, S. Lee, W. I. Park, S. Kim, L. Liu, U. Paik, *Nano Res.* **2015**, *7*, 491.
[146] Z. Haifeng, R. Weina, C. Chuanwei, *Nanotechnology* **2015**, *26*, 274002.
[147] C. Wang, L. Wu, H. Wang, W. Zuo, Y. Li, J. Liu, *Adv. Funct. Mater.* **2015**, *25*, 3524.
[148] J. Zhang, K. Wang, Q. Xu, Y. Zhou, F. Cheng, S. Guo, *ACS Nano* **2015**, *9*, 3369.
[149] S. H. Choi, J.-H. Lee, Y. C. Kang, *ACS Nano* **2015**, *9*, 10173.